Solution Structure of the Luzopeptin-DNA Complex†

Xiaolu Zhang and Dinshaw J. Patel*

Department of Biochemistry and Molecular Biophysics, College of Physicians and Surgeons, Columbia University, New York, New York 10032

Received October 16, 1990; Revised Manuscript Received January 15, 1991

ABSTRACT: The luzopeptin-d(C-A-T-G) complex (1 drug/duplex) has been generated in aqueous solution and its structure characterized by a combined application of two-dimensional NMR experiments and molecular dynamics calculations. One equivalent of luzopeptin binds to the self-complementary tetranucleotide duplex with the 2-fold symmetry of the antitumor agent and the DNA oligomer retained on complex formation. We have assigned the exchangeable and nonexchangeable proton resonances of luzopeptin and the d(C-A-T-G) duplex in the complex and identified the intermolecular proton-proton NOEs that define the alignment of the antitumor agent at its binding site in duplex DNA. The analysis was greatly aided by a large number of intermolecular NOEs involving exchangeable protons on both the luzopeptin and the DNA in the complex. The molecular dynamics calculations were guided by 140 intramolecular nucleic acid distance constraints, 74 intramolecular luzopeptin distance constraints, and 96 intermolecular distance constraints between luzopeptin and the nucleic acid protons in the complex. The quinoline rings of luzopeptin bisintercalate at d(C-A)·d(T-G) steps in the d(C-A-T-G) duplex and sandwich two Watson-Crick A·T base pairs between the bisintercalation site. The long axis of the quinoline rings are collinear with the long axis of the flanking Watson-Crick C1·G4 and A2·T3 base pairs such that the OCH_3-6 group is directed toward the C1-A2 step and the OH-3 group is directed toward the T3-G4 step in the complex. The quinoline chromophore stacks with purines on both strands, with the quinoline A ring stacked on A2 and the quinoline B ring stacked on G4 in the complex. The C1·G4 and A2·T3 base pairs that flank the intercalation sites are parallel to each other with partial overlap of T3 and G4 in the T3-G4 step but no overlap of C1 and A2 in the C1-A2 step in the complex. The cyclic depsipeptide ring of luzopeptin is positioned in the minor groove of the d(C-A-T-G) duplex with the oligopeptide and oligonucleotide chains running antiparallel to each other. The cyclic depsipeptide backbone of luzopeptin exhibits cis peptide bonds at Pyr-Gly and Gly-Sar steps in the luzopeptin-d(C-A-T-G) complex in solution, in contrast to all trans peptide bonds for free luzopeptin in the crystalline state. The formation of cis peptide bonds for luzopeptin in the complex results in an increased separation of the long sides of the rectangular cyclic depsipeptide backbone and reorients the glycine amide proton so that it can form an intermolecular hydrogen bond with the 2-carbonyl of T3 in the complex. This observation explains, in part, the requirement for Watson-Crick A·T pairs to be sandwiched between the quinolines at the bisintercalation site in the luzopeptin-DNA complex. Further, the trans ester carbonyl group of the Ser-meVal step located on the short sides of the rectangular cyclic depsipeptide backbone of luzopeptin forms an intermolecular hydrogen bond with the exposed 2-amino proton of G4 in the complex. This observation explains the requirement for Watson-Crick G·C pairs to flank the bisintercalation site in the luzopeptin-DNA complex. We also detect van der Waals contacts between the protons and CH_3 groups of luzopeptin and the minor-groove sugar faces and base-pair edges of the nucleic acid in the luzopeptin-d(C-A-T-G) complex. The complementary intermolecular contacts between the cyclic depsipeptide backbone extends over much of the potential interacting surface of the complex. The Cα protons of Pyr, Gly, and Sar are directed toward the interior of the cyclic depsipeptide ring of luzopeptin and this hydrophobic patch interacts with the minor-groove edge of adjacent Watson-Crick A2·T3 base pairs in the complex. Our NMR studies on the luzopeptin-d(C-A-T-G) complex unequivocally establish that antitumor agents can undergo conformational transitions on complex formation with DNA, and it is the conformation of the drug in the complex that should serve as the starting point for drug design studies. The above structural details on the solution structure of the luzopeptin-DNA complex also explain the sequence selectivity of luzopeptin for bisintercalation at d(C-A)·d(T-G) steps in the d(C-A-T-G) duplex in solution.

Luzopeptin, **1**, is an actinoleukin-like antibiotic isolated from fermentation broths of an aerobic strain of actinomycete (Ohkuma et al., 1980; Tomita et al., 1980). It contains two identical substituted quinoline chromophores that are linked to a cyclic decadepsipeptide containing a 2-fold element of symmetry (Konishi et al., 1981; Arnold & Clardy, 1981). The cyclic depsipeptide contains an unusual cyclic amino acid possessing a tetrahydropyridazine moiety. The antitumor activity of luzopeptin has been demonstrated in a range of animal tumor systems (Rose et al., 1983).

Viscometric and fluorimetric binding studies of luzopeptin to closed circular DNA established that the antitumor drug complexes through bisintercalation (Huang et al., 1980, 1982, 1983) in a manner similar to the related antibiotic echinomycin (Waring & Fox, 1983; Wang et al., 1984; Gao & Patel, 1988, 1989b). Enzymatic footprinting with DNase I and micrococcal

† This research was funded in part by Columbia University start-up funds and in part by NIH CA-46778. The NMR spectrometers were purchased from funds donated by the Robert Woods Johnson Jr. Trust and Matheson Trust toward setting up the NMR center in the Basic Medical Sciences at Columbia University.

0006-2960/91/0430-4026$02.50/0

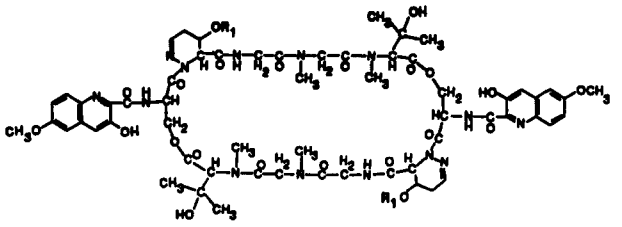

1

nuclease demonstrated a sequence preference for luzopeptin binding at alternating A and T residues on duplex DNA (Fox et al., 1988).

The structure of luzopeptin has been solved in the crystalline state (Arnold & Clardy, 1981) along with an NMR characterization of the antitumor agent in organic solvents (Searle et al., 1988a). The luzopeptin cyclic depsipeptide backbone in the crystal adopts a rectangular shape with the long sides consisting of twisting antiparallel β-extended chains stabilized by weak glycine amide to glycine carbonyl hydrogen bonds. The two substituted quinoline chromophores project from the same face of the cyclic decadepsipeptide backbone in the crystal and can potentially sandwich either two or three base pairs at the bisintercalation site in the complex (Arnold & Clardy, 1981).

Structural studies on luzopeptin–DNA complexes to date are restricted to a solution NMR study of the luzopeptin–d(G-C-A-T-G-C) complex (1 drug/duplex) where two-dimensional nonexchangeable proton data sets in D_2O were analyzed to identify structural features of the bisintercalation site (Searle et al., 1989). Our NMR studies have focused on the luzopeptin complex with d(C-A-T-G) **2** (1 drug/duplex) in H_2O and D_2O solution. These studies combine two-dimensional NMR and molecular dynamics computations to define the solution structure of the luzopeptin–d(C-A-T-G) complex **3**. There are important differences between the earlier qualitative model of the luzopeptin–d(G-C-A-T-G-C) complex (Searle et al., 1989) and our quantitative characterization of the luzopeptin–d(C-A-T-G) complex in aqueous solution.

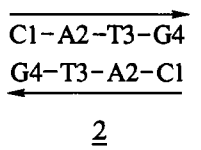

2

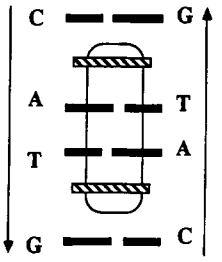

3

Materials and Methods

Oligonucleotide Synthesis. The d(C-A-T-G) tetranucleotide was synthesized on a Beckman System 1 plus DNA synthesizer by the solid-phase cyanoethyl phosphoramidite method. The crude 5′-dimethoxytritylated tetranucleotide was isolated by treatment of the support with concentrated aqueous ammonia for 45 h at room temperature. The tetranucleotide was then purified by reverse-phase HPLC in two stages and desalted on a Sephadex G-25 column. The oligomer was finally converted to sodium form on a Dowex 50X8 cation-exchange column.

Luzopeptin–Oligonucleotide Complex. Luzopeptin was provided by Dr. M. Konishi of the Bristol-Myers Research Institute, Tokyo, Japan. About 2 equiv of solid luzopeptin was directly added to 0.45 mL of the d(C-A-T-G) duplex in aqueous buffer solution (0.1 M NaCl, 10 mM phosphate, and 0.1 mM EDTA). The mixture was diluted to 5 mL with water and shaken in a cold room for 24 h. The solution was then lyophilized and redissolved in 0.45 mL of H_2O. The excess luzopeptin that was insoluble was removed by centrifugation.

The luzopeptin–d(C-A-T-G) complex (concentration 4.5 mM) was adjusted to an uncorrected glass electrode pH reading of 7.35 with dilute NaOH or HCl. For experiments in H_2O, the complex was lyophilized and then redissolved in 0.45 mL of 90% H_2O/10% D_2O. For experiments in D_2O, the complex was first lyophilized, redissolved in 99.8% D_2O, and relyophilized. This procedure was repeated three times with the complex finally dissolved in 0.45 mL of 99.96% D_2O under nitrogen gas.

NMR Experiments. All NMR spectra were recorded on Bruker AM 500 or AM 400 spectrometers. Quadrature detection was used in both dimensions with the carrier frequency placed on the H_2O resonance for all experiments. All data sets were transferred to a VAX 11-780 or a micro VAX II computer and processed with the FORTRAN program FTNMR provided by Dr. Dennis Hare (Hare Research). The FIDs for the initial t_1 value in each 2D data set were multiplied by 0.5 in order to eliminate t_1 ridge artifacts.

Two-dimensional data sets on the complex in D_2O buffer were recorded on a Bruker AM 500 spectrometer. The sample temperature was 40 ± 0.5 °C. The spectral width was 4500 Hz (9 ppm). Continuous low-power irradiation of the residual water signal was applied during the recycle time for all spectra. The COSY spectrum in D_2O was collected with 1024 complex points in t_2, 350 complex free induction decays (FIDs) in t_1, 128 transients for each FID, and a repetition delay of 1.3 s. Both time-domain data sets were multiplied by a 0° phase-shifted sine bell window function. A set of NOESY spectra with mixing times of 75 and 150 ms was recorded with 1024 complex points in t_2, 400 complex FIDs in t_1, 128 transients for each FID, and a repetition delay of 1.3 s. Both time-domain data sets were multiplied by a 70° phase-shifted sine bell window function.

The COSY spectrum of the complex in H_2O was acquired with 2048 complex points in t_2, 256 complex points in t_1, and 128 transients for each FID. The relaxation time was 1.5 s. The sample temperature was set to 45 ± 0.5 °C. The spectral width was 4500 Hz (9 ppm). The NOESY spectrum of the complex in H_2O was recorded without irradiation of the water signal. The water signal was suppressed by a jump and return water suppression pulse sequence as the detection pulse. The pulse sequence used in this experiment is

$$[t_0 - 90° - t_1 - 90° - t_m - (90°_x - \Delta - 90°_{-x}) - t_2]_n \quad (1)$$

The relaxation time t_0 was 1.2 s. The mixing time t_m was 150 ms. The delay Δ was set to 80 μs to optimize the excitation in imino, amino, aromatic, and amide proton regions of the complex spectrum. The spectrum was collected with 96 transients for each FID, 1024 complex points in t_2, and 350 complex points in t_1. The sample temperature was set to 25 ± 0.5 °C. The spectral width was 8400 Hz (21 ppm).

Interproton Distance Constraints. The cross peaks in a NOESY spectrum represent dipole–dipole couplings between nuclei that are within 5 Å of each other. The intensities of these NOE cross peaks provide information about the internuclear distance based on the relationship

$$\text{NOE} \propto f(\tau_c)\frac{1}{r^6} \quad (2)$$

where $f(\tau_c)$ is a function of the correlation time τ_c and represents the influence of the motion of the molecule on the

observed NOE. The correlation time τ_c can be defined as the average time for a molecule to rotate by 1 rad for reorientational motion. The correlation time of a molecule in solution will be affected by the molecular size, temperature, and viscosity of the solution. In principle, given a known distance r_{kl}, the unknown distance r_{ij} can be directly calculated from

$$r_{ij} = r_{kl}\left(\frac{\mathrm{NOE}_{kl}}{\mathrm{NOE}_{ij}}\right)^{1/6} \quad (3)$$

where NOE_{kl} and NOE_{ij} are the NOEs between atoms k and l and atoms i and j, respectively. However, the validity of eqs 2 and 3 is limited. First, eq 2 is valid only for two-spin relaxation or direct magnetization transfer, while in practice NOE cross peaks result from multispin relaxation. The assumption that NOEs result only from direct magnetization transfer will be valid only for NOEs measured from NOESY spectra recorded with extremely short mixing times. Unfortunately, signal-to-noise ratios are usually quite poor at short mixing times. Studies have shown that the effect of indirect magnetization transfer can cause significant errors for estimation of distances from NOESY spectra. Borgias and James (1988) have quantitatively estimated the errors caused by ignoring indirect magnetization transfer, and they indicate that the errors for a calculated distance of 3-Å range from ±0.50 Å in a 50-ms NOESY spectrum to ±0.80 Å in a 250-ms NOESY spectrum.

Second, the $f(\tau_c)$ term in eq 2 can be canceled in eq 3 only under the assumption that the molecule tumbles as a rigid isotropic unit where all interproton vectors have the same effective correlation times. In most cases, macromolecules are not rigid bodies, and internal motions in the molecule cause different effective correlation times for different interproton vectors. The errors caused by using the second assumption have been estimated to be ~10% in calculated distances (Lane, 1988; Borgias & James, 1988).

The volume integrals of individual NOE cross peaks in the luzopeptin–d(C-A-T-G) complex were measured from NOESY contour plots recorded with a mixing time of 75 ms in D_2O and 150 ms in H_2O solution. Since eq 3 is only valid when the effective correlation times of the i–j and k–l interproton vectors are the same, the reference distances in the calculation of the unknown interproton distances have to be chosen appropriately. In the case of oligonucleotides, the fixed distances corresponding to sugar H2′–H2″ and cytidine H5–H6 can be used as the reference distances. NMR studies of DNA oligomers have shown that the effective correlation times of sugar H2′–H2″ vectors are significantly shorter than those of the cytidine H5–H6 vectors (Clore & Gronenborn, 1984; Gronenborn & Clore, 1985; Gronenborn et al., 1984). Considering that the contribution from internal motion to the effective correlation times of the sugar–sugar and sugar–base distances will mainly be dominated by motion within the sugar units, while that of the base–base will mainly be dominated by motion about the glycosidic bond, it has been suggested that all unknown distances involving sugar–sugar and sugar–base vectors, except sugar H1′–base vectors, should be calculated by using r[H2′–H2″] as a reference and all those involving base–base and sugar H1′–base vectors should be calculated by using r[C(H5)–C(H6)] as a reference. In this work, we used the r[H2′–H2″] distance of 1.8 Å as a reference distance in the calculation of the unknown interproton distances involving sugar–sugar and sugar–base vectors in DNA, except the sugar H1′–base vector. The r[C(H5)–C(H6)] distance of 2.45 Å was used as a reference distance in the calculation of the unknown interproton distances involving base–base and sugar H1′–base vectors in DNA. The geminal r[CαH–CαH] distance of 1.8 Å on the luzopeptin sarcosine residue was used as a reference distance in the calculation of all unknown interproton distances for luzopeptin in the complex.

It has been recently suggested that r[C(H5)–C(H6)] should be used as the reference for estimating proton–proton distances for all pairs in DNA oligomer duplexes (Nerdal et al., 1988; Reid et al., 1989). However, it should be noted that, on the basis of r[C(H5)–C(H6)] as the reference distance, we calculate r[H2′–H2″] to be 2.25 Å (averaged), which is 0.45 Å longer than the actual fixed distance of 1.8 Å.

The intermolecular proton–proton distances defined by lower and upper bounds for the luzopeptin–d(C-A-T-G) complex listed in Tables VI and VII were estimated by using r[C(H5)–C(H6)] as the reference distance.

The approach we used for calculation of distances is based on the assumptions discussed above and leads to errors in the calculated distances. Thus, each input distance constraint is defined by upper and lower bounds, with the true distance nested within the bounds. The upper and lower bounds were set to $d \pm 0.8$ Å (where d is the calculated distance) for NOESY data collected in D_2O and $d \pm 1.0$ Å for NOESY data collected in H_2O. These ranges for the bounds should be free from the errors caused by ignoring indirect magnetization transfer and internal motions of the molecule.

For a methyl group, the protons were replaced by a pseudoatom located in the center of the three methyl protons, and the upper bound was modified by adding a correction term of 1.0 Å. This corresponds to the distance between the pseudoatom and any one of the three methyl protons. In the case where methylene protons are not stereospecifically assigned, a correction term corresponding to the maximum possible error was added to the upper bound. This correction term is simply the distance between the methylene protons (1.8 Å).

Structure Computations. Initial model building and structural analysis were carried out on an Evans & Sutherland PS390 color graphics system interfaced to a VAX 780 computer using MACROMODEL (Professor W. Clark Still, Columbia University) and INSIGHT programs (Biosym Technologies, Inc). All energy minimization and molecular dynamics calculations were carried out on a CONVEX C2 computer using the program XPLOR (Professor Axel Brunger, Yale University) in which all hydrogen atoms are treated explicitly. The total energy used for the energy minimizations and molecular dynamics calculations can be grouped into the empirical energy and effective energy. The empirical energy functions were taken from Brooks et al. (1983) and include covalent and nonbonded restraint terms. The effective NOE restraint potential, E_{NOE}, has the form of a square well (Clore et al., 1986):

$$\begin{aligned} E_{\mathrm{NOE}} &= k_{\mathrm{NOE}}(r_{ij} - r_{ij}^{+})^2 && \text{if } r_{ij} > r_{ij}^{+} \\ &= 0 && \text{if } r_{ij}^{-} < r_{ij} < r_{ij}^{+} \\ &= k_{\mathrm{NOE}}(r_{ij} - r_{ij}^{-})^2 && \text{if } r_{ij} < r_{ij}^{-} \end{aligned} \quad (4)$$

where r_{ij}^{+} and r_{ij}^{-} are the upper and lower limits for the NOE-derived distance, respectively. r_{ij} is the distance calculated from the current calculated structures. k_{NOE} is the scale factor used for the NOE restraint potential in units of kilocalories per mole per square angstrom. Bond lengths involving hydrogen atoms were kept fixed with the SHAKE algorithm (Ryckaert et al., 1977).

Each of the initial structures was first subjected to 300 cycles of energy minimization in order to relieve bad contacts between nonbonded atoms. During this energy minimization, the hydrogen-bond contraints for DNA base pairs were used to retain

Table I: Nucleic Acid Proton Chemical Shifts in the Luzopeptin–d(C-A-T-G) Complex (1 Drug/Duplex)[a]

	chemical shifts (ppm)										
	NH	NH_2	H8	H2	H6	H5/CH_3	H1′	H2′,2″	H3′	H4′	H5′,5″
C1		7.68			7.55	5.48	5.31	2.20, 2.36	4.60	3.94	3.78, 3.88
A2			8.09	7.65			5.95	2.72, 2.79	4.98	4.44	4.21, 3.84
T3	12.86				6.95	1.42	5.62	2.15, 2.37	4.61	3.71	4.09, 4.08
G4	11.52		7.83				5.92	2.29, 2.56	4.63	4.03	4.14

[a] 0.1 M NaCl, 10 mM phosphate, and 0.1 mM EDTA in aqueous solution. Exchangeable proton chemical shifts in H_2O, pH 7.35, at 25 °C. Nonexchangeable proton chemical shifts in D_2O, pH 7.35, at 40 °C.

Watson–Crick pairing in the DNA oligomer duplex. Another 300 cycles of restrained energy minimization with a scale factor of 2 in the NOE effective potential term was applied after inputting all NOE distance constraints derived from NOESY spectra. The structure was then subjected to molecular dynamics refinements in two stages, namely, high-temperature stage and cooling/equilibration stage. In the high-temperature stage, integration of the Newton equations of motion was performed by a Verlet integration algorithm (Verlet, 1967) with initial velocities assigned to a maxwell distribution at 300 K. A loop with 10 cycles was used to gradually introduce the NOE restraints by increasing the NOE scale factor. The time step was set to be 0.0004 ps, and 250-step dynamics were run for each NOE scale factor. The system was heated up without rescaling the velocities of the atoms at the end of each 250-step dynamics calculation, unless the temperature of the system exceeded 8000 K. In the cooling/equilibration stage, the NOE scale factor was set to be 32. The integration of the Newton equations of motion was also performed by a Verlet integration algorithm with initial velocities assigned to a Maxwell distribution at 300 K. The temperature of the system was maintained at 300 K by rescaling the velocities of the atoms every 0.250 ps. The time step of the integrator was 0.001 ps. The structure was then further refined by restrained energy minimization. The structure was repeatedly refined by using combined restrained energy minimization and restrained molecular dynamics, until no single distance violation was greater than 0.1 Å.

Results

Stoichiometry and Symmetry of Complex. The luzopeptin–d(C-A-T-G) complex was generated following addition of 1 equiv of luzopeptin to the d(C-A-T-G) duplex. The proton NMR parameters establish that the complex retains the 2-fold element of symmetry inherent in its individual components luzopeptin and the d(C-A-T-G) duplex. This is reflected in the exchangeable proton (5.5–14.0 ppm) and nonexchangeable proton (1.0–9.0 ppm) spectra of the luzopeptin–d(C-A-T-G) complex (1 drug/duplex) in 0.1 M NaCl and 10 mM phosphate aqueous buffer as shown in Figure S1, panels A and B, respectively (see supplementary material). The proton resonances in the complex are narrow and amenable to characterization by two-dimensional NMR studies in H_2O and D_2O solution.

Exchangeable Nucleic Acid Protons in Complex. The exchangeable proton spectrum of the luzopeptin–d(C-A-T-G) complex in H_2O buffer, pH 7.35, at 25 °C (Figure S1A) exhibits two exchangeable imino protons at 11.52 and 12.86 ppm and an additional exchangeable resonance at 10.20 ppm. The imino and amino nucleic acid protons have been assigned following analysis of the NOESY (150-ms mixing time) contour plot of the complex recorded in H_2O buffer, pH 7.35, 25 °C (Figure S2, supplementary material).

Expanded regions of the NOESY contour plot establishing distance connectivities from the 9.6–13.0 ppm imino and exchangeable protons to the 5.0–8.6 ppm amino and H1′ protons and to the 1.2–5.0 ppm H2′,2″ and CH_3 protons are plotted in Figure 1, panels A and B, respectively. The cross-peak assignments are listed in the figure caption. The observed cross peaks permit correlation of guanosine imino with the hydrogen-bonded and exposed cytidine amino protons (peaks E and F, Figure 1B) within the C1·G4 pair and correlation of the thymidine imino with the adenosine H2 proton (peak C, Figure 1B) within the A2·T3 pair in the complex. It should be noted that we do not detect an NOE between the imino protons of flanking C1·G4 and A2·T3 pairs in the NOESY spectrum of the complex (Figure S2). The imino and amino nucleic acid proton assignments in the luzopeptin–d(C-A-T-G) complex at 25 °C are listed in Table I.

Table II: Luzopeptin Proton Chemical Shifts in the Luzopeptin–d(C-A-T-G) Complex (1 Drug/Duplex)[a]

D-Serine		β-Hydroxy-*N*-methylvaline	
NH	8.37	NCH_3	3.37
CαH	5.72	CαH	5.13
$C\beta H_2$	4.25, 4.66	$C\gamma H_3$	1.20, 1.52
Pyridazine		Sarcosine	
CαH	5.18	NCH_3	2.98
CβH	5.70	$C\alpha H_2$	4.28, 5.51
$C\gamma H_2$	2.53, 2.65	Quinoline	
CδH	7.35	OH-3	10.20
$COCH_3$	2.02	H4	7.00
Glycine		H5	6.55
NH	8.09	OCH_3-6	3.68
$C\alpha H_2$	4.78	H7	6.09
		H8	6.09

[a] 0.1 M NaCl, 10 mM phosphate, and 0.1 mM EDTA in aqueous solution. Exchangeable proton chemical shifts in H_2O, pH 7.35, at 45 °C. Nonexchangeable proton chemical shifts in D_2O, pH 7.35, at 40 °C.

Exchangeable Luzopeptin Protons in Complex. The exchangeable protons are located at the amide groups of D-Ser and Gly as well at the OH-3 position on the quinoline ring of luzopeptin. These luzopeptin exchangeable protons have been assigned in the complex from the observed cross-peak patterns in NOESY and COSY data sets recorded in H_2O solution. Thus, the 10.20 ppm resonance exhibits a very strong NOE to the H4 quinoline proton (peak 1, Figure 1B) and must be assigned to the OH-3 quinoline proton in the complex.

We can identify and distinguish between the D-Ser and Gly amide protons by recording COSY spectra of the complex in H_2O solution at 45 °C. Thus, the amide proton at 8.37 ppm exhibits a coupling connectivity to the Cα proton at 5.72 ppm (Figure S3A, supplementary material), which in turn exhibits connectivities to Cβ protons at 4.25 and 4.66 ppm, permitting assignment of the 8.37 ppm exchangeable resonance to the amide proton of D-Ser in the complex. The remaining amide proton at 8.09 ppm must be assigned to Gly in the complex and exhibits a coupling connectivity to the superimposed Cα protons at 4.78 ppm (Figure S3A). The antitumor agent proton assignments in the luzopeptin–d(C-A-T-G) complex at 45 °C are listed in Table II.

Nonexchangeable Nucleic Acid Protons in Complex. There is excellent resolution of resonances in the nonexchangeable

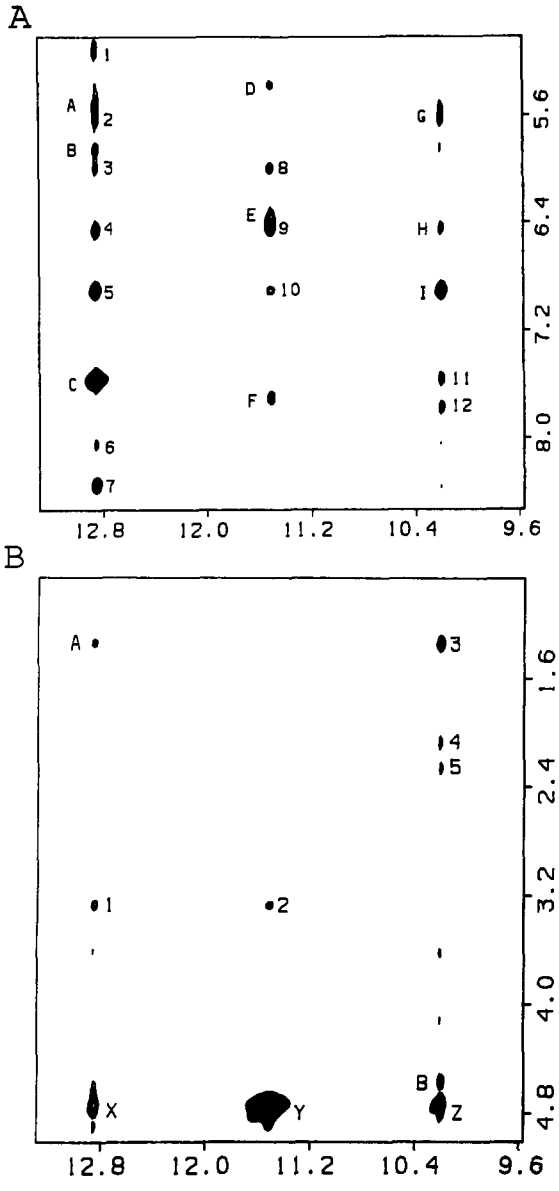

FIGURE 1: Expanded NOESY contour plots (mixing time 150 ms) of the luzopeptin–d(C-A-T-G) complex in 0.1 M NaCl and 10 mM phosphate buffer in H_2O, pH 7.35, at 25 °C. (A) Contour plots correlating the 9.6–13.0 ppm imino and aromatic OH proton region with the 5.0–8.6 ppm proton region. The intramolecular NOE cross peaks A–I are assigned as follows: A, T3(NH3)–T3(H1′); B, T3(NH3)–A2(H1′); C, T3(NH3)–A2(H2); D, G4(NH1)–C1(H5); E, G4(NH1)–C1($NH_2$4e); F, G4(NH1)–C1($NH_2$4hb); G, Qui(OH-3)–Ser(CαH); H, Qui(OH-3)–Qui(H5); I, Qui(OH-3)–Qui(H4). The intermolecular NOE cross peaks 1–12 are assigned as follows: 1, T3(NH3)–Pyr(CαH); 2, T3(NH3)–Ser(CαH); 3, T3(NH3)–Qui(H7/H8); 4, T3(NH3)–Qui(H5); 5, T3(NH3)–Qui(H4); 6, T3(NH3)–Gly(NH); 7, T3(NH3)–Ser(NH); 8, G4(NH1)–Qui(H7/H8); 9, G4(NH1)–Qui(H5); 10, G4(NH1)–Qui(H4); 11, Qui(OH-3)–A2(H2); 12, Qui(OH-3)–G4(H8). (B) Contour plots correlating the 9.6–13.0 ppm imino and aromatic OH proton region with the 1.2–5.0 ppm region. The intramolecular cross peaks A and B are assigned as follows: A, T3(NH3)–T3(CH_3); B, Qui(OH-3)–Ser(CβH). The exchangeable proton to H_2O cross peaks X–Z are assigned as follows: X, H_2O–T3(NH3); Y, H_2O–G4(NH1); Z, H_2O–Qui(OH-3). The intermolecular cross peaks 1–5 are assigned as follows: 1, T3(NH3)–Val(NCH_3); 2, G4(NH1)–Val(NCH_3); 3, Qui(OH-3)–T3(CH_3); 4, Qui(OH-3)–T3(H2′); 5, Qui(OH-3)–T3(H2″).

proton spectrum of the luzopeptin–d(C-A-T-G) complex in D_2O buffer, pH 7.35, at 40 °C (Figure S1B). The nonexchangeable nucleic acid protons have been assigned following analysis of the NOESY (Figure S4, supplementary material) and COSY (Figure S5, supplementary material) contour plots

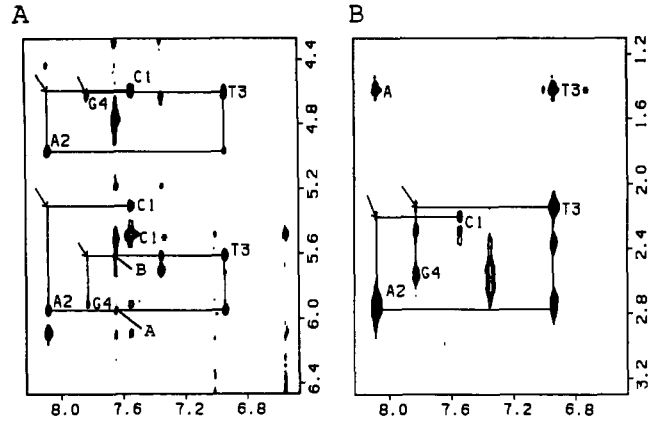

FIGURE 2: Expanded NOESY (mixing time 150 ms) contour plots of the luzopeptin–d(C-A-T-G) complex in 0.1 M NaCl and 10 mM phohsphate buffer in D_2O, pH 7.35, at 40 °C. (A) Contour plots correlating the base protons (6.6–8.2 ppm) with the sugar H1′ and H3′ protons (4.4–6.4 ppm). The cytidine H6–H5 NOE is designated by an asterisk. The lines trace the distance connectivities between base and sugar H1′ protons. The arrows point to absent NOEs between the H8 of A2 and the H1′ (and H3′) of C1 and absent NOEs between the H8 of G4 and the H1′ (and H3′) of T3. The cross peaks A and B are assigned as follows: A, A2(H2)–A2(H1′); B, A2-(H2)–T3(H1′). (B) Contour plot correlating the base protons (6.8–8.2 ppm) with the sugar H2′,2″ and CH_3 protons (1.2–3.2 ppm). The thymidine H6-CH_3 NOE is designated by an asterisk. The lines trace the distance connectivities between base and sugar H2′ protons. The arrows indicate weak NOEs between the H8 of A2 and the H2′ of C1 and weak NOEs between the H8 of G4 and H2′ of T3. The cross peak A is assigned to the NOE between the H8 of A2 and the CH_3 of T3.

in D_2O buffer. The cross peaks are well resolved in NOESY contour plots recorded at 25 and 40 °C (Figure S4, panels A and B, respectively) and can be analyzed by sequential assignment procedures (Hare et al., 1983).

The distance connectivities in the expanded NOESY contour plot (150-ms mixing time) between the base protons (6.8–8.2 ppm) and the sugar H1′ (5.2–6.0 ppm) and H3′ (4.5–5.1 ppm) in the complex at 40 °C is plotted in Figure 2A. One can trace the chain from C1 to G4 by monitoring the NOEs between the base (purine H8 or pyrimidine H6) protons and their own and 5′-flanking sugar H1′ protons (and sugar H3′ protons). We note that the NOE between the H8 proton of A2 and the H1′ (and H3′) proton of C1, as well as the NOE between the H8 proton of G4 and the H1′ (and H3′) proton of T3, is absent (designated by arrows) in the complex (Figure 2A). We detect an NOE between the H8 of A2 and the CH_3 of T3 (peak A, Figure 2B) in the A2-T3 step in the complex. Further, NOEs are detected between the H2 proton of A2 and its own H1′ proton (peak A, Figure 2A) and the H1′ proton of T3 (peak B, Figure 2A) on the same strand but not to the H1′ proton of G4 on the partner strand in the complex.

The distance connectivities in the expanded NOESY contour plot (150-ms mixing time) between the base protons (6.8–8.2 ppm) and the sugar H2′,2″ protons (2.0–2.8 ppm) in the complex at 40 °C is plotted in Figure 2B. The chain can be traced from C1 to G4 by noting the NOEs between the base (purine H8 or pyrimidine H6) protons and their own and 5′-flanking sugar H2′ (Figure 2B) and H2″ protons. We note that these connectivities are weak for C1-A2 and T3-G4 steps (designated by arrows in Figure 2B) in the complex.

These base and sugar H1′, H2′,2″, and H3′ proton assignments can be confirmed following analysis of other regions of the NOESY contour plots of the complex. Expanded COSY (Figure S3B) contour plots correlating H1′ (5.2–6.0 ppm) and H3′ (4.5–5.0 ppm) protons with the H2′,2″ (2.1–2.9 ppm)

exhibit well-resolved cross peaks with the assignments listed in Figure S3B. The sugar H4′ protons and some sugar H5′,5″ protons can be assigned in an analogous manner by monitoring through-space and through-bond connectivities in the complex. Thus, we detect well-resolved coupling connectivities between the H3′ and H4′ protons in the COSY spectrum of the complex (peaks E, F, G, and H, Figure S5B; assignments listed in figure caption). The base and sugar nucleic acid nonexchangeable proton assignemnts in the luzopeptin–d(C-A-T-G) complex at 40 °C are listed in Table I.

Nonexchangeable Luzopeptin Protons in Complex. We have already outlined the assignments of the D-Ser and Gly protons of luzopeptin in the complex based on connectivities from the amide to the Cα protons and in the case of D-Ser to the Cβ protons in two-dimensional spectra recorded in H_2O solution. The nonexchangeable protons on the sarcosine (Sar), β-hydroxy-*N*-methylvaline (Val), pyridazine (Pyr), and quinoline (Qui) residues of luzopeptin in the luzopeptin–d(C-A-T-G) complex have been assigned following analysis of the NOESY and COSY data sets in D_2O solution.

The protons on the pyridazine moiety can be assigned by following through-bond connectivities along the CαH–CβH–$C\gamma H_2$–CδH spin system as reflected in cross peaks for CαH–CβH (peak C), CβH–CγHA (peak D), CγHA–CγHB (peak E), CγHB–CδH (peak B), and CδH–CβH (peak A) proton pairs in the COSY contour plot (Figure S5A).

We detect a strong coupling cross peak between the geminal sarcosine $C\alpha H_2$ protons at 4.28 and 5.51 ppm in the complex (peak A, Figure S5B). The CH_3 resonance at 2.98 ppm is assigned to the NCH_3 of sarcosine since NOEs are detected to both $C\alpha H_2$ protons of the same residue.

The upfield CH_3 resonances at 1.20 and 1.52 ppm are assigned to the nonequivalent $C\gamma H_3$ groups of β-hydroxy-*N*-methylvaline in the complex. Both $C\gamma H_3$ resonances exhibit strong NOEs to the proton at 5.13 ppm, which is assigned to the CαH proton of Val in the complex. The three-proton singlet at 3.37 ppm is assigned to the NCH_3 of β-hydroxy-*N*-methylvaline since we detect NOEs to the CαH and $C\gamma H_3$ protons on the same residue. We have been unable to locate the OH proton of β-hydroxy-*N*-methylvaline in the complex.

The quinoline protons are assigned as follows: H4 (7.00 ppm), H5 (6.55 ppm), and H7, H8 (6.09 ppm) with partial resolution of the H7 and H8 protons at 50 °C. We detect a strong NOE cross peak between the H4 and H5 protons but do not detect a COSY cross peak reflecting the four bonds that separate these protons. The quinoline OCH_3 group at 3.68 ppm exhibits strong NOEs to the H5 and H7 protons on the same residue. Finally, the 10.20 ppm quinoline OH-3 exchangeable proton exhibits a very strong NOE to H4 and a weak NOE to H5 quinoline protons in the complex.

This completes the assignment of the nonexchangeable luzopeptin protons in the luzopeptin–d(C-A-T-G) complex, and the chemical shifts at 40 °C are listed in Table II.

Intermolecular Contacts between Luzopeptin and DNA. Our ability to assign the DNA oligomer (Table I) and luzopeptin (Table II) protons in the luzopeptin–d(C-A-T-G) complex has permitted the identification and characterization of intermolecular drug–DNA NOEs in NOESY spectra recorded in H_2O and D_2O solution. A set of 48 intermolecular contacts in one symmetrical half of the complex was identified in 150-ms mixing time NOESY spectra recorded in H_2O solution at 25 °C and 75-ms NOESY spectra recorded in D_2O solution at 40 °C. The intermolecular NOEs in the complex involving exchangeable protons are numbered in Figure 1 and listed in the figure caption, and those involving nonexchangeable protons are numbered in Figure 3 and listed in the figure caption. A complete list of intermolecular NOEs is given in Tables III and IV.

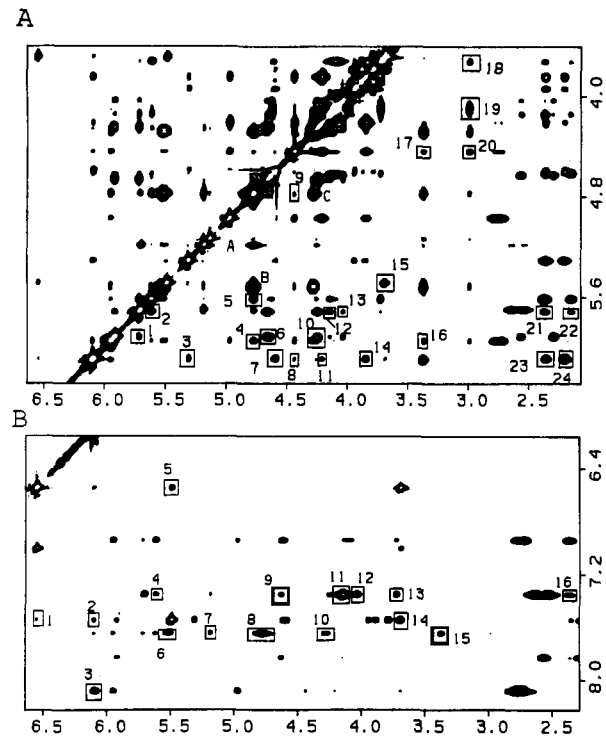

FIGURE 3: Expanded NOESY (mixing time 150 ms) contour plots of the luzopeptin–d(C-A-T-G) complex in 0.1 M NaCl and 10 mM phosphate buffer in D_2O, pH 7.35, at 40 °C. (A) Contour plots correlating the 2.0–6.7 ppm region with the 3.6–6.4 ppm region. The cross peaks 1–24 are assigned as follows: 1, G4(H1′)–Ser(CαH); 2, T3(H1′)-Ser(CαH); 3, C1(H1′)-Qui(H8); 4, A2(H1′)-Gly($C\alpha H_2$); 5, T3(H1′)-Gly($C\alpha H_2$); 6, G4(H1′)-Ser(CβH); 7, C1(H3′)-Qui(H7); 8, A2(H4′)-Qui(H8); 9, A2(H4′)-Gly($C\alpha H_2$); 10, G4(H1′)-Ser(CβHB); 11, A2(H5′)-Qui(H8); 12, G4(H5′)-Ser(CαH); 13, G4(H4′)-Ser(CαH); 14, A2(H5″)-Qui(H8); 15, C1(H5)-Qui(OCH_3-6); 16, A2(H1′)-Val(NCH_3); 17, A2(H4′)-Val(NCH_3); 18, T3(H4′)-Sar(NCH_3); 19, T3(H5′)-Sar(NCH_3); 20, A2(H4′)-Sar(NCH_3); 21, C1(H2″)-Ser(CαH); 22, C1(H2′)-Ser(CαH); 23, C1(H2″)-Qui(H8); 24, C1(H2′)-Qui(H7). The cross peaks A–C are assigned as follows: A, Gly($C\alpha H_2$)-Pyr(CαH); B, Gly($C\alpha H_2$)-Sar(CαHA); C, Gly($C\alpha H_2$)-Sar(CαHB). (B) Contour plots correlating the 2.0–6.7 ppm region with the 6.2–8.2 ppm region. The cross peaks 1–16 are assigned as follows: 1, C1(H6)-Qui(H5); 2, C1(H6)-Qui(H7); 3, A2(H8)-Qui(H7); 4, T3(H1′)-Pyr(CδH); 5, G4(H3′)-Pyr(CδH); 6, A2(H2)-Sar(CαHA); 7, A2(H2)-Pyr(CαH); 8, A2(H2)-Gly($C\alpha H_2$) 9, G4(H3′)-Pyr(CδH); 10, A2(H2)-Sar(CαHB); 11, G4(H5′)-Pyr(CδH); 12, G4(H4′)-Pyr(CδH); 13, T3(H4′)-Pyr(CδH); 14, C1(H6)-Qui(OCH_3-6); 15, A2(H2)-Val(NCH_3); 16, T3(H2″)-Pyr(CδH).

Table III: Intermolecular NOEs between Luzopeptin Quinoline Protons and DNA Tetramer Protons in the Luzopeptin–d(C-A-T-G) Complex

luzopeptin quinoline protons	DNA protons		
	minor groove	helix axis	major groove
OH-3		T3(NH3)	T3(CH_3)
H4		T3(NH3), G4(NH1)	C1($NH_2$4)
H5		G4(NH1)	C1($NH_2$4, H5)
OCH_3-6			C1($NH_2$4, H5, H6)
H7			A2(H8, H5′, H5″) C1(H6, H2′, H3′)
H8	A2(H1′, H4′)		

The observed intermolecular NOEs between the quinoline ring protons and the base protons of both the C1·G4 and A2·T3 base pairs (Table III) establishes that the quinoline rings bisintercalate at symmetry-related (C1-A2)·(T3-G4)

Table IV: Intermolecular NOEs between Luzopeptin Depsipeptide Ring Protons and DNA Tetramer Protons in the Luzopeptin–d(C-A-T-G) Complex

luzopeptin depsipeptide protons	DNA protons		
	minor groove	helix axis	major groove
D-Ser(NH)	A2(H2)	T3(NH3)	
D-Ser(CαH)	T3(H1′, H2′, H2″) G4(H1′, H4′, H5″)		
D-Ser(CβH)	G4(H1′)		
Pyr(CαH)	A2(H2)		
Pyr(CδH)	T3(H1′, H2″, H4′) G4(H4′, H5″)		G4(H3′)
Gly(NH)	A2(H2), T3(H1′)	T3(NH3)	
Gly(CαH)	A2(H2, H1′), T3(H1′)		
Sar(NCH_3)	A2(H1′, H4′)		
Sar(CαH)	A2(H2, H1′)		
L-*N*-meVal(NCH_3)	A2(H2, H1′, H4′)		

steps in the d(C1-A2-T3-G4) duplex. The long axis of the quinoline has the OH-3, H4, H5, and OCH_3-6 protons along one edge, while the H7 and H8 protons line the other edge of the intercalating chromophore. We detect intermolecular NOEs between the OH-3, H4, H5, and OCH_3-6 protons and protons located along the helix axis (imino protons) and base protons located in the major groove (purine H8, pyrimidine H6, H5, CH_3-5, and NH_2-4) (Table III). These NOEs establish that this polar edge of the quinoline, which extends from the OH-3 proton to the OCH_3-6 group, is directed toward the major groove, and these observations permit alignment of the long axis of the quinoline with the long axis of the flanking C1·G4 and A2·T3 base pairs in the complex. The quinoline H8 proton exhibits intermolecular NOEs to the sugar H1′ and H4′ protons of A2, establishing that this edge of the intercalating chromophore is directed toward the minor groove in the complex. Finally, the quinoline H7 proton is directed toward the C1-A2 sugar–phosphate backbone on the basis of the observed NOEs between this proton and the base and sugar protons of C1 and A2 in the complex (Table III). The above patterns of intermolecular NOEs involving the quinoline protons identify the intercalation site and define its sequence specificity and, in addition, establish the orientation of the intercalated quinoline rings with respect to the flanking base pairs.

The intermolecular NOEs between the protons on the cyclic depsipeptide ring of luzopeptin and the d(C-A-T-G) duplex in the complex are listed in Table IV. These luzopeptin protons exhibit intermolecular contacts to the tetranucleotide minor-groove protons, establishing unequivocally that luzopeptin bisintercalates through the minor groove and positions its depsipeptide ring in this groove of the helix. We outline below the intermolecular contacts between individual residues in the depsipeptide and the complementary segment on the d(C-A-T-G) duplex in the complex.

The pattern of intermolecular NOEs exhibited by the amide, CαH, and CβH_2 protons of D-Ser define the orientation of this residue relative to the intercalation site on the DNA helix. The D-Ser amide proton exhibits intermolecular NOEs to the H2 proton of A2 and the imino proton of T3 and intermolecular NOEs to the H8 quinoline proton and the NCH_3 proton of L-*N*-meVal in the complex. These data require that the D-Ser amide proton be in the plane of the quinoline ring and be directed inward and toward the opposite face of the cyclic depsipeptide backbone. The D-Ser CαH proton exhibits NOEs to the minor-groove sugar protons of T3 and G4 and hence must be directed toward the sugar–phosphate backbone of the T3-G4 step that defines the intercalation site. The Ser CβH_2 protons are also directed toward the DNA backbone but

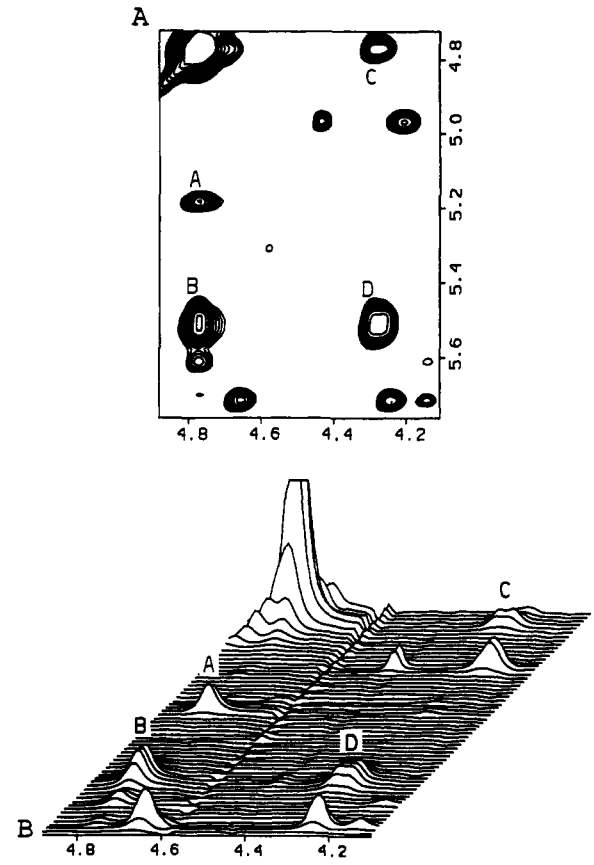

FIGURE 4: Expanded NOESY (mixing time 75 ms) contour plots correlating the 4.0–5.0 ppm region with the 4.7–5.7 ppm region in the luzopeptin-d(C-A-T-G) complex in 0.1 M NaCl and 10 mM phosphate buffer in D_2O, pH 7.35, at 40 °C. (A) Contour plot and (B) stacked plot. The cross peaks A–D are assigned as follows: A, Pyr(CαH)-Gly(CαH); B, Gly(CαH)-Sar(CαHA); C, Gly(CαH)-Sar(CαHB); D, Sar(CαHA)-Sar(CαHB).

contact primarily the G4 sugar residue.

The cyclic pyridazine moiety is an unusual feature of the luzopeptin structure. It has protons distributed at the CαH, CβH, CγH_2, and CδH positions on the ring and an $OCOCH_3$ side chain attached to the Cβ position. The observed intermolecular NOE between the CαH proton of pyridazine and the H2 proton of A2 establishes that this pyridazine proton is directed inward and toward the minor-groove edge of the A2 base in the complex. We also detect intermolecular NOEs between the CδH prydazine proton and the sugar protons of T3 (H1′, H2″, and H4′) and G4 (H3′, H4′, and H5′) in the complex (Table IV). These NOEs align the pyridazine CδH proton toward the sugar–phosphate backbone at the T3-G4 step spanning the intercalation site in the complex. The observation of a strong NOE cross peak from the pyridazine CαH proton to the superpositioned Gly CαH_2 protons (peak A, Figure 4, panels A and B) establishes formation of a cis peptide bond linking the pyridazine and Gly residues of luzopeptin in the complex.

The Gly amide and CαH_2 protons of luzopeptin exhibit intermolecular NOEs to the base and minor-groove sugar protons of A2 and T3 on the d(C-A-T-G) duplex. These results require that the amide and one or both CαH_2 protons of Gly be directed toward the A2-T3 step in the minor groove so that the Gly amide can be positioned to form potential intermolecular hydrogen bonds in the complex. The Gly CαH_2 protons are superpositioned on each other and are partially resolved only on raising the temperature of the complex. By contrast, the Sar CαH_2 protons exhibit a 1.2 ppm separation

Table V: Distance Bounds between Luzopeptin Exchangeable and Nonexchangeable Protons in the Complex and Their Comparison with Observed Distances in the NMR–Molecular Dynamics Refined Structure of the Complex

intermolecular proton pairs	distance bounds (Å)	actual distance (Å)	intermolecular proton pairs	distance bounds (Å)	actual distance (Å)	intermolecular proton pairs	distance bounds (Å)	actual distance (Å)
Qui(OH-3)–Qui(H4)	2.0–3.7	2.2	Pyr(CαH)–Pyr(CβH)	2.0–3.1	2.6	Gly(NH)–Pyr(CαH)	2.0–3.8	3.7
Qui(H4)–Qui(H5)	2.0–3.3	2.5	Pyr(CαH)–Gly(CαHB)	2.0–3.2	2.3	Gly(NH)–Gly(CαHA)	2.0–3.9	2.4
Qui(H4)–Qui(OCH_3-6)	2.8–5.3	4.6	Pyr(CβH)–Gly(CαHA)	2.0–3.8	3.7	Gly(NH)–Gly(CαHB)	2.0–3.9	3.0
Qui(H5)–Qui(OCH_3-6)	2.0–3.6	2.2	Pyr(CβH)–Pyr(CγHA)	2.0–3.2	2.5	Gly(NH)–Sar(CαHA)	2.0–4.0	3.6
Qui(H8)–Val(NCH_3)	2.0–3.9	2.2	Pyr(CβH)–Pyr(CγHB)	2.0–3.2	2.4	Sar(NCH_3)–Val($C\gamma H_3A$)	2.0–5.2	2.9
Qui(H7)–Qui(OCH_3-6)	3.2–5.7	4.2	Pyr($OCOCH_3$)–Val(CαH)	2.0–3.5	3.6	Sar(CαHA)–Sar(CαHB)	1.9–2.9	1.8
Ser(NH)–Qui(H8)	2.2–4.2	3.1	Pyr(CδH)–Pyr(CγHA)	2.0–3.2	2.6	Sar(CαHA)–Val(NCH_3)	2.0–3.6	1.9
Ser(NH)–Ser(CαH)	2.0–4.0	2.9	Pyr(CδH)–Pyr(CγHB)	2.0–3.2	2.6	Val(NCH_3)–Val(CαH)	2.1–4.6	3.6
Ser(NH)–Ser(CβHA)	2.0–4.0	2.9	Gly(CαHA)–Sar(CαHA)	1.9–2.9	2.0	Val(NCH_3)–Val($C\gamma H_3A$)	2.2–4.7	3.3
Ser(NH)–Val(NCH_3)	2.0–4.1	2.6	Gly(CαHA)–Sar(CαHB)	2.0–3.1	2.2	Val(NCH_3)–Val($C\gamma H_3B$)	2.0–4.9	2.6
Ser(CαH)–Ser(CβHA)	2.0–3.1	2.7	Gly(CαHA)–Sar(N-CH_3)	2.0–4.5	4.5	Val(NCH_3)–Sar(CαHB)	2.0–3.5	3.4
Ser(CαH)–Ser(CβHB)	2.0–3.1	2.4	Gly(CαHA)–Val(N-CH_3)	2.0–3.8	3.6	Val($C\gamma H_3A$)–Val($C\gamma H_3B$)	2.0–4.5	2.3
Ser(CβHA)–Ser(CβHB)	1.8–2.8	1.8						

Table VI: Distance Bounds between Luzopeptin and d(C-A-T-G) Nonexchangeable Protons in the Complex and Their Comparison with Observed Distances in the NMR–Molecular Dynamics Refined Structure of the Complex

intermolecular proton pairs	distance bounds (Å)	actual distance (Å)	intermolecular proton pairs	distance bounds (Å)	actual distance (Å)	intermolecular proton pairs	distance bounds (Å)	actual distance (Å)
C1(H5)–Qui(H5)	2.9–4.4	3.6	A2(H1′)–Gly(CαHA)	2.5–5.0	3.8	T3(H2″)–Pyr(CδH)	2.3–3.8	2.7
C1(H2′)–Qui(H7)	2.0–3.0	1.9	A2(H1′)–Sar(NCH_3)	2.4–4.9	3.1	T3(H4′)–Pyr(CδH)	2.9–4.4	3.5
C1(H6)–Qui(H7)	3.9–5.0	4.6	A2(H4′)–Sar(NCH_3)	2.5–5.0	3.9	T3(H1′)–Pyr(CδH)	3.5–5.0	3.8
C1(H3′)–Qui(H7)	2.3–3.8	3.3	A2(H1′)–Sar(CαHA)	3.2–4.7	3.3	T3(H1′)–Gly(CαHA)	2.5–5.0	4.6
C1(H5)–Qui(OCH_3-6)	2.0–3.4	2.6	A2(H4′)–Val(NCH_3)	2.6–5.0	3.0	G4(H1′)–Ser(CαH)	2.7–4.2	3.7
C1(H6)–Qui(OCH_3-6)	2.4–3.9	2.5	A2(H2)–Val(NCH_3)	2.6–5.0	3.0	G4(H5″)–Ser(CαH)	2.1–3.6	2.7
A2(H1′)–Qui(H8)	2.7–4.2	4.2	A2(H1′)–Val(NCH_3)	2.9–5.0	3.4	G4(H4′)–Ser(CαH)	2.5–4.0	2.6
A2(H8)–Qui(H7)	2.6–4.1	3.4	A2(H2)–Sar(CαHB)	3.2–4.7	4.8	G4(H4′)–Pyr(CδH)	2.0–3.5	2.1
A2(H5″)–Qui(H7)	2.0–3.5	2.0	A2(H4′)–Qui(H8)	3.5–5.0	4.0	G4(H5″)–Pyr(CδH)	2.0–3.5	2.8
A2(H5′)–Qui(H7)	2.5–4.0	2.7	T3(H1′)–Ser(CαH)	2.3–3.8	3.4	G4(H3′)–Pyr(CδH)	3.4–4.9	4.0
A2(H2)–Pyr(CαH)	3.4–4.9	4.3	T3(H2″)–Ser(CαH)	2.6–4.1	3.1	G4(H1′)–Ser(CβHA)	2.1–3.6	2.4
A2(H2)–Gly(CαHA)	2.2–5.0	3.0	T3(H2′)–Ser(CαH)	3.0–4.5	3.7			

in the complex. The superpositioned Gly $C\alpha H_2$ protons exhibit NOEs to the H2 proton of A2 and the sugar H1′ protons of A2 and T3 and therefore must be directed inward and toward the minor-groove edge of the A2-T3 step in the complex. The observation of strong cross peaks from the superpositioned Gly $C\alpha H_2$ protons to the resolved Sar $C\alpha H_2$ protons (peaks B and C, Figure 4, panels A and B) establishes formation of a cis peptide bond linking the Gly and Sar residues of luzopeptin in the complex.

A set of intermolecular NOEs are detected from the Sar NCH_3 and $C\alpha H_2$ protons to the base and sugar protons of A2, defining the intermolecular contacts in the complex. The Sar NCH_3 protons exhibit NOEs to the minor-groove sugar protons of A2 and hence this group must be directed inward and toward the sugar–phosphate backbone at the A2 step in the complex. The Sar $C\alpha H_2$ protons exhibit NOEs to the H2 base and sugar H1′ protons of A2 and hence must be directed inward and toward the minor-groove edge of the A2 base in the complex. We do not detect a strong NOE between the CαH proton of L-*N*-meVal and either of the $C\alpha H_2$ protons of Sar, establishing a trans orientation of the peptide bond linking these luzopeptin residues in the complex.

We detect intermolecular NOEs from the NCH_3 proton of L-*N*-meVal to the base H2 and minor-groove sugar protons of A2 and intramolecular NOEs to the H8 quinoline proton and the amide proton of D-Ser in the complex. These data require that the NCH_3 group be in the plane of the quinoling ring and be directed inward and toward the opposite face of the cyclic depsipeptide backbone. Indeed, the D-Ser amide, the NCH_3 group of L-*N*-meVal, and the H8 quinoline proton are aligned in a triangular arrangement in the plane defined by the aromatic ring of the intercalating quinoline chromophore. This pattern of NOEs is consistent with a trans alignment of the peptide bond linking the quinoline and D-Ser residues of luzopeptin in the complex. The absence of any intermolecular NOEs involving the CαH proton of L-*N*-meVal suggests that this proton be directed outward from the cyclic depsipeptide ring and also away from the sugar–phosphate backbone in the complex. The observed NOEs between the NCH_3 and $C\beta H_3$ protons of L-*N*-meVal require formation of a nonpolar patch with the CH_3 groups aligned on the same face of the luzopeptin in the complex. There are no NOEs that define the alignment of the ester bond that links the D-Ser and L-*N*-meVal residues so that the ester bond can adopt either cis or trans geometry, and further, the carbonyl functionality can be directed either toward or away from the DNA.

Experimental Distance Bounds. We have outlined under Materials and Methods the approach used to define lower and upper bounds for proton pairs with a detectable NOE between them in the NOESY spectra at short mixing times of the luzopeptin–d(C-A-T-G) complex. The volume integrals for NOE cross peaks were measured for a NOESY data set on the complex recorded at a mixing time of 75 ms in D_2O solution and a related NOESY data set on the complex recorded at a mixing time of 150 ms in H_2O solution. A set of distance bounds corresponding to the 37 intramolecular distance constraints within the luzopeptin ring is listed in Table V, and a set corresponding to the 48 intermolecular distance constraints in the luzopeptin–d(C-A-T-G) complex is listed in Tables VI and VII. These 48 intermolecular distance bounds along with 70 constraints between nucleic acid protons and 37 constraints between luzopeptin protons in the complex were incorporated in the molecular dynamics simulation and correspond to a total of 155 constraints for one symmetrical half of the luzopeptin–d(C-A-T-G) complex.

Starting Models for Structure Refinement. Two quite different initial structures of the complex were generated for the molecular dynamics computations as a test for the con-

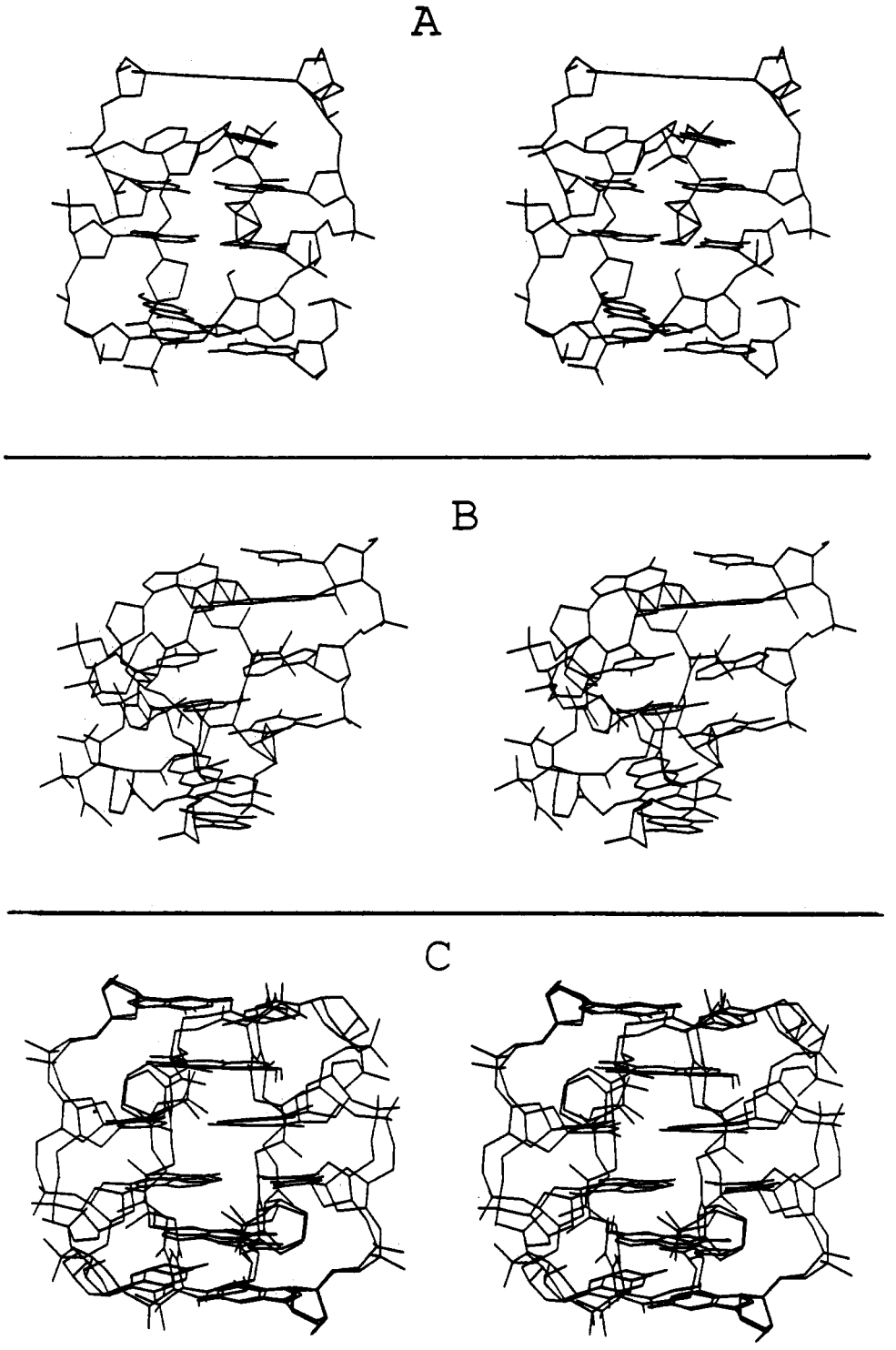

FIGURE 5: Stereoviews of the initial and refined structures of the luzopeptin–d(C-A-T-G) complex used as starting models in the molecular dynamics refinements with NMR distance constraints. (A) Init-A structure. The tetranucleotide duplex was genrated by using MACROMODEL starting from B-form DNA with intercalation sites incorporated at symmetry-related d(C-A)·d(T-G) steps. The luzopeptin was built with all trans peptide and ester bonds by using MACROMODEL, and the quinolines were aligned so that they insert into the intercalation sites. (B) Init-B structure. The DNA geometry at the intercalation site corresponds to that in the nogalamycin–DNA complex in solution (Zhang & Patel, 1990). The X-ray structure of luzopeptin was used without modification of the desipeptide backbone but with realignment of the quinolines so that they insert into the intercalation sites. (C) A stereoview of two superpositioned structures of the luzopeptin–d(C-A-T-G) complex following molecular dynamics refinement including NMR-based distance constraints. These refined structures were generated from Init-A and Init-B starting structures.

vergence characteristics of the final structures. One starting structure (Init-A) was generated as follows: The d(C-A-T-G) duplex was built from B-form DNA by using MACROMODEL, and symmetrically related intercalation sites were generated by separating the C1·G4 and A2·T3 base pairs. The luzopeptin was built with all trans peptide and ester linkages by using MACROMODEL, and the quinoline rings were positioned for intercalation such that their chromophores can sandwich two base pairs. The luzopeptin was docked onto the d(C-A-T-G) duplex such that the cyclic depsipeptide backbone of luzopeptin was located in the minor groove and the quinoline rings were bisintercalated at (C-A)·(T-G) steps in the d(C-A-T-G) duplex. A stereo view of the Init-A starting structure is shown in Figure 5A.

Table VII: Distance Bounds between Luzopeptin and d(C-A-T-G) Exchangeable Protons in the Complex and Their Comparison with Observed Distances in the NMR–Molecular Dynamics Refined Structure of the Complex

intermolecular proton pairs	distance bounds (Å)	actual distance (Å)
C1($NH_2$4)–Qui(H4)	2.0–4.0	3.0
C1($NH_2$4)–Qui(H5)	2.0–3.8	3.0
C1($NH_2$4)–Qui(OCH_3-6)	2.0–3.9	3.9
A2(H2)–Ser(NH)	2.0–3.6	3.4
A2(H2)–Gly(NH)	2.0–4.0	3.4
T3(H1′)–Gly(NH)	2.0–4.0	3.5
T3(NH3)–Qui(OH-3)	2.0–3.7	3.5
T3(NH3)–Ser(NH)	2.5–4.5	4.5
T3(NH3)–Gly(NH)	2.3–4.3	4.1
T3(NH3)–Qui(H4)	2.0–3.9	3.6
T3(CH_3)–Qui(OH-3)	2.0–4.9	3.6
G4(NH1)–Qui(H4)	2.2–4.2	3.9
G4(NH1)–Qui(H5)	2.0–4.0	3.8

The second starting structure (Init-B) was generated as follows: The structure of the d(C-A-T-G) duplex corresponds to this segment in the recently determined structure of the nogalamycin-d(A-G-C-A-T-G-C-T) complex (2 drugs/duplex) in solution. We have established that nogalamycin intercalation sites occur at symmetry-related (C-A)·(T-G) steps in the d(C-A-T-G) segment of the octanucleotide duplex (Zhang & Patel, 1990). The X-ray structure of luzopeptin with all trans peptide and ester bonds (Arnold & Clardy, 1981) was used without modification of the depsipeptide backbone but with realignment of the quinolines so that they can insert into the intercalation sites separated by two base pairs. The stereoview of the Init-B starting structure in Figure 5B shows the luzopeptin docked in the minor groove with the quinolines intercalating at (C-A)·(T-G) steps on the d(C-A-T-G) duplex. The Init-A (Figure 5A) and the Init-B (Figure 5B) starting structures of the complex have very high van der Waals energy at the level of 10^8 kcal and are strikingly different as apparent from a root-mean-square deviation of 3.4 Å for all heavy atoms between these structures.

Structure Refinement. The initial structures served as starting models for structure refinement using molecular dynamics (MD) computations with NMR-based distance bounds as input constraints. The refinement protocol is outlined under Materials and Methods and was judged to be complete when no single distance violation was greater than 0.2 Å. The final structures that were refined from two quite different starting structures are superimposed on the basis of a best fit for all heavy atoms in Figure 5C and exhibit a root-mean-square deviation of 1.0 Å.

One of these final structures for the luzopeptin–d(C-A-T-G) complex is plotted in stereo with emphasis on different views in Figure 6. The intermolecular interproton distances measured for this structure of the complex show good agreement with the input experimental distance bounds used in the molecular dynamics calculation (Tables VI and VII).

Structural Features of NMR–MD Refined Complex. The luzopeptin–d(C-A-T-G) complex (1 drug/duplex) exhibits 2-fold symmetry with the quinoline rings intercalated at symmetry-related (C1-A2)·(T3-G4) steps. Stereoviews of the complex are plotted in Figure 6. The view looking into the major groove is plotted in Figure 6A. The cyclic depsipeptide ring is positioned in the minor groove with views normal to the helix axis in Figure 6B and down the minor-groove direction in Figure 6C. The complementary fit between the DNA minor-groove surface and the cyclic depsipeptide surface is emphasized in Figure 6B. The stacking alignment between the quinoline ring and flanking base pairs is shown in Figure 7A, and the intercalation site is shown in Figure 7B.

A striking feature of the luzopeptin–d(C-A-T-G) complex in solution is the conformation of the luzopeptin (Figures 8B and S6B), which differs significantly from that reported in the crystal for free luzopeptin (Figures 8A and S6A) (Arnold & Clardy, 1981). Indeed, the luzopeptin structure in the complex exhibits two cis peptide bonds at the Pyr-Gly and Gly-Sar steps (Figure S7B, supplementary material) in contrast to all trans peptide bonds for the free drug in the crystalline state (Figure S7A, supplementary material). The differences are discussed further below.

Luzopeptin Conformation in Complex. The luzopeptin conformation in the complex in solution exhibits several distinct features outlined below. The depsipeptide backbone adopts a rectangular shape with the corners defined by the Cα atom of L-*N*-meVal and the Cβ atom of D-Ser. The two quinoline rings project out from one face of the rectangle, are parallel to each other, and are separated by 10.2 Å (Figure 8B).

The amide proton of D-Ser and the NCH_3 proton of L-*N*-meVal are in the same plane as the quinoline ring, with these protons and the quinoline H8 proton aligned in a triangular arrangement. The CαH_2 protons of Gly and Sar and the CαH proton of Pyr project inward within the rectangular arrangement, while the Sar NCH_3, pyridazine ring, the CαH and CβH_2 protons of D-Ser, and the CγH_3 and CβOH protons of L-*N*-meVal project outward from the rectangular arrangement.

The pyridazine CαH proton is positioned opposite the CαH_2 protons of Gly and Sar across the rectangular arrangement of the cyclic depsipeptide backbone. The two glycine CαH_2 protons are differentiated as follows: The HA proton is on the same side and the HB proton is on the opposite side of the glycine amide proton. The two sarcosine CαH_2 protons are differentiated as follows: The CαHA proton is on the same side and the CαHB proton is on the opposite side of the NCH_3 group of the adjacent L-*N*-meVal residue.

The average plane of the pyridazine ring is parallel to the plane of the rectangular arrangement of the depsipeptide ring. The CαH and CβH pyridazine protons adopt equatorial alignments, with the Cβ-$OCOCH_3$ group in an axial alignment and on the face pointing away from the DNA helix.

The amide proton of Gly and the NCH_3 group of L-*N*-meVal project normal to the rectangular plane in the same direction as the quinoline rings. This positions the amide group of Gly for hydrogen bonding to acceptors on the base-pair edges of the minor groove of the d(C-A-T-G) duplex in the complex.

The peptide bonds linking Sar and L-*N*-meVal and linking D-Ser and Pyr, as well as the ester bond linking L-*N*-meVal and D-Ser, adopt a trans alignment. By contrast, the peptide bonds linking Pyr and Gly and linking Gly and Sar adopt a cis alignment (Figure S7B). The Gly-Sar peptide bond remains parallel to but protrudes out from the rectangular arrangement of the depsipeptide backbone (Figure S7B).

The carbonyl group of the Sar-meVal amide linkage projects out from the rectangular face away from the DNA binding site, while the carbonyl group of the Pyr-Gly amide linkage and the carbonyl group of the meVal-Ser ester linkage project out from the rectangular face toward the DNA binding site. Finally, the Ser-Qui amide carbonyl group is in the plane and directed inward within the cyclic depsipeptide ring.

There are no cross-strand hydrogen bonds for the luzopeptin structure in the complex due to the separation between the long sides of the rectangular arrangement of the backbone (Figure 8B).

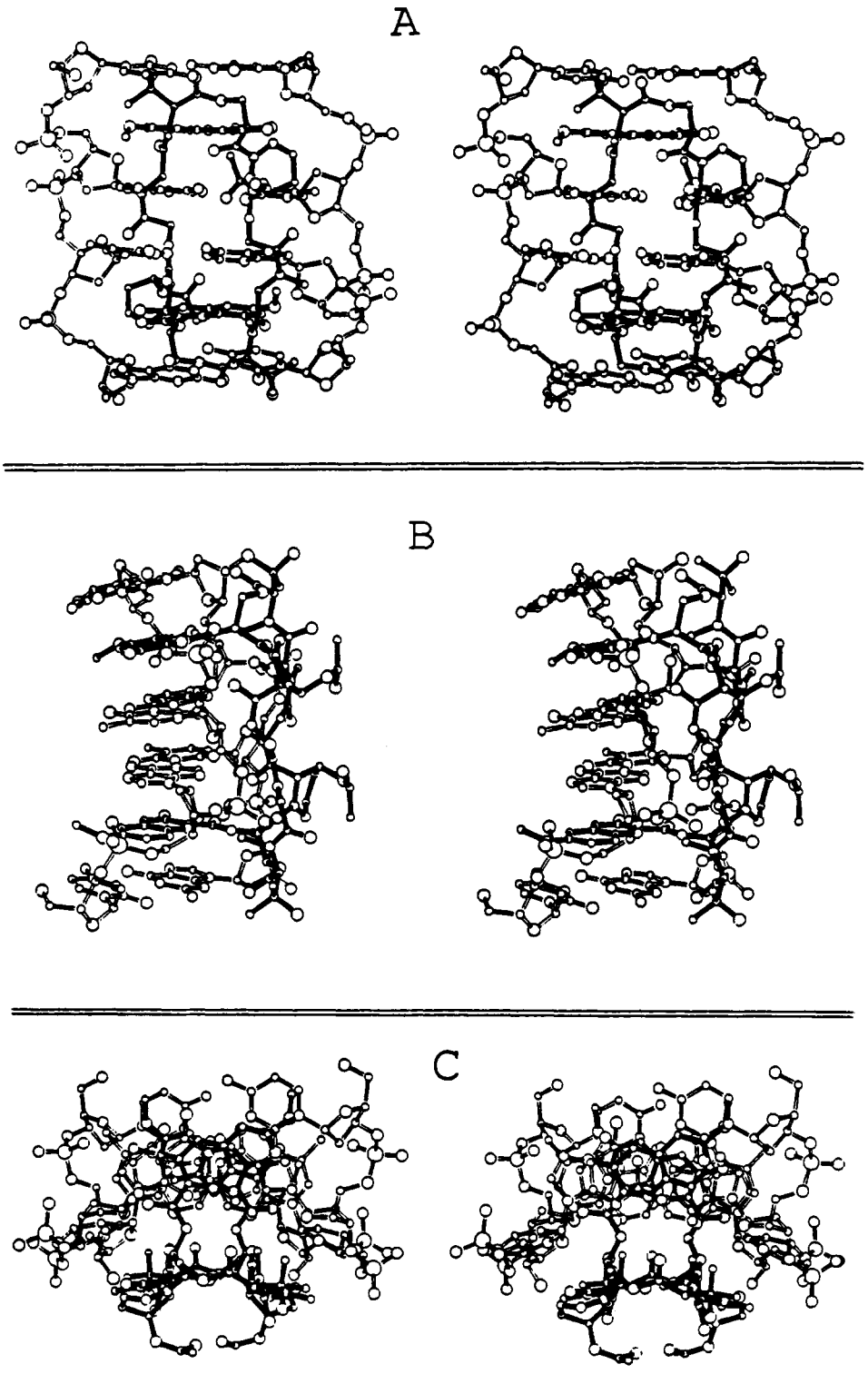

FIGURE 6: Stereoviews of the luzopeptin–d(C-A-T-G) complex. (A) View looking into the major groove. (B) View emphasizes the complementary fit between the cyclic decadepsipeptide and the sugar–phosphate backbone in the minor groove of DNA. (C) View down the helix axis emphasizes the positioning of the cyclic decadepsipeptide in the minor groove of the duplex.

DNA Conformation in the Complex. A qualitative examination of the experimental NOE data establishes that the A·T and G·C pairs adopt Watson–Crick alignments and the glycosidic torsion angles are in the anti range in the luzopeptin–d(C-A-T-G) complex. These features are an integral part of the NMR–MD solution structure of the complex.

Conformational features of the (C1-A2)·(T3-G4) intercalation site in the complex are of special interest. We note that the C1·G4 and A2·T3 base pairs are parallel to each other in the luzopeptin–d(C-A-T-G) complex (Figure 7B), and the increased separation between these base pairs is reflected in the interproton separations between the base protons and the 5′-flanking sugar H1′ and H3′ protons at the C1-A2 and T3-G4 steps centered about the intercalation site in the complex. Thus, the A2(H8) to C1(H1′) and C1(H3′) proton separations are 6.9 and 4.4 Å, respectively, while the G4(H8) to T3(H1′) and T3(H3′) proton separations are 7.4 and 6.3 Å, respectively.

We note partial stacking of T3 and G4 in the T3-G4 step but no stacking of C1 and A2 in the C1-A2 step, resulting in some shearing of the base pairs at the (C1-A2)·(T3-G4) intercalation site in the complex (Figures 7A and S8A). This

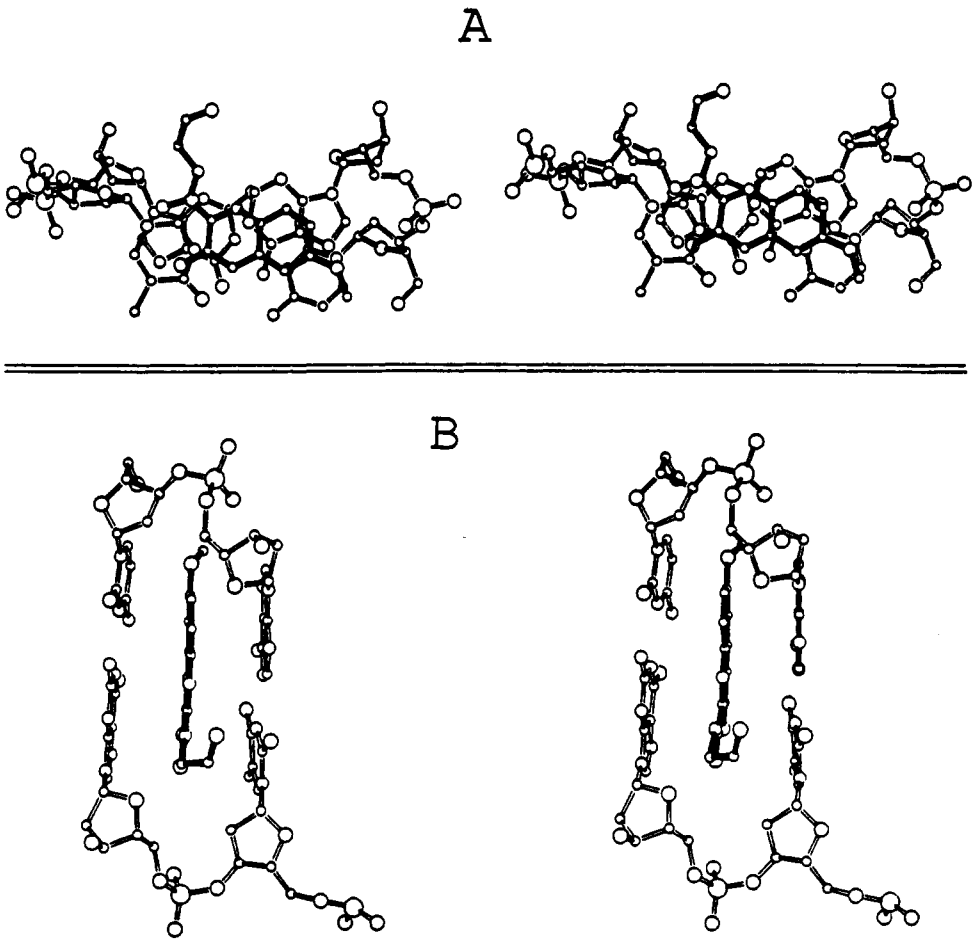

FIGURE 7: Stereoviews of the intercalation site (drug quinoline chromophore and adjacent base pairs) in the luzopeptin–d(C-A-T-G) complex. (A) This view emphasizes the overlap geometry between the quinoline ring and flanking base pairs. (B) This view emphasizes the parallel alignment of the base pairs at the intercalation site.

shearing is in the same direction but not as large as that observed for the same intercalation site in the nogalamycin complex (Figure S8B), where the C·G and A·T base pairs are significantly buckled at the intercalation site (Zhang & Patel, 1990).

We detect a right-handed helical alignment at the A2-T3 step sandwiched between intercalation sites in the NMR–MD structure of the complex. This observation is consistent with the directionality of the observed NOEs between the H6 proton of T3 and 5′-flanking sugar H1′,H2′,2″, and H3′ protons of A2 as well as the NOE between the H8 proton of A2 and the CH_3 of T3 (peak A, Figure 2B) in the complex.

There is a widening of the minor groove in the luzopeptin–d(C-A-T-G) complex. The cross-strand P–P separation is 17.1 Å at the intercalation site and is 17.4 Å between A2-T3 phosphates on partner strands.

Overlap Geometry at the Intercalation Sites. The alignment of the quinoline chromophore and the overlap geometries with respect to the flanking C1·G4 and A2·T3 base pairs in the NMR–MD refined structure reflects the intermolecular NOEs observed experimentally between the quinoline and nucleic acid residues defining the intercalation site (Table III). The long axis of the quinoline ring is aligned collinearly with the long axis of the base pairs such that the OCH_3-6 group is directed toward the C1-A2 step and the OH-3 group is directed toward the T3-G4 step in the complex (Figure 7A). This alignment positions the quinoline H4 and H5 protons in the major groove, while the quinoline H8 proton is positioned in the minor groove. The quinoline chromophore stacks with purines on both strands, with the quinoline A ring stacked on A2 and the quinoline B ring stacked on G4 in the complex (Figure 7A).

Intermolecular Contacts in the Minor Groove. We observe a complementary fit between the cyclic depsipeptide backbone of luzopeptin and the widened minor groove of the d(C-A-T-G) tetranucleotide duplex in the NMR-MD-refined structure of the complex (Figure 6B). The long axis of the cyclic depsipeptide backbone, which starts at the D-Ser Cβ atom and proceeds through the pyridazine, glycine, and sarcosine functionalities to the *N*-meVal Cα atom is aligned antiparallel to the d(C1-A2-T3-G4) sugar–phosphate backbone in the complex (Figure 9).

We note that the cis Gly-Pyr peptide linkage projects out from the mean plane of the cyclic depsipeptide backbone such that both the pyridazine carbonyl and glycine amide groups are directed toward the minor groove of the DNA (Figure S7B). The glycine amide proton forms an intermolecular hydrogen bond (1.91 Å) with the 2-carbonyl group of T3 and along with its symmetry-related partner anchors the center of the complex.

The ester functionality linking the D-Ser and L-*N*-meVal residues is located on the short axis of the rectangular-shaped cyclic depsipeptide backbone. The carbonyl group of the ester is directed toward the minor groove and forms an intermolecular hydrogen bond (1.94 Å) with the 2-amino group of G4 and along with its symmetry-related partner anchors the ends of the complex.

A set of intermolecular van der Waals contacts are observed to stabilize the structure of the NMR–MD-refined structure of the luzopeptin–d(C-A-T-G) complex in solution (Figure 9). The D-Ser CαH proton is directed toward the T3-G4 step and

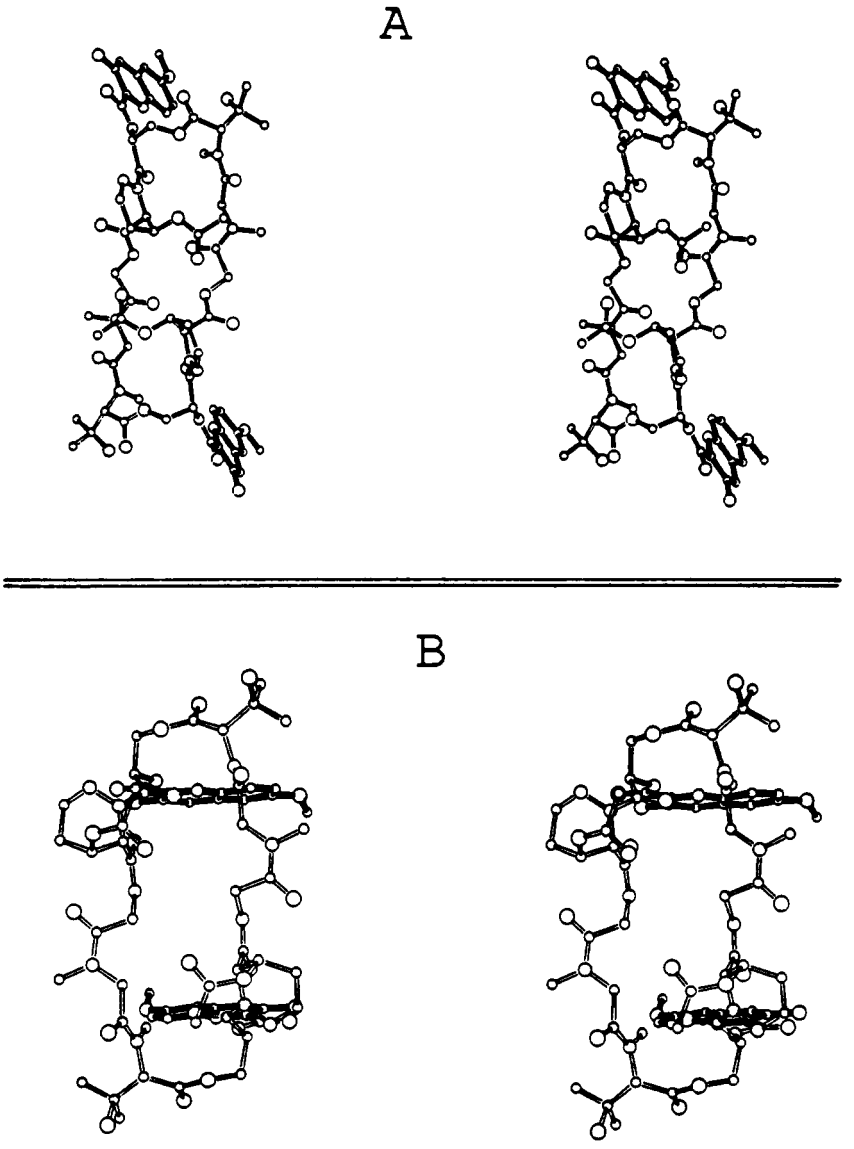

FIGURE 8: Stereoviews of the luzopeptin conformation for (A) the free drug in the crystalline state (Arnold & Clardy, 1981) and (B) the luzopeptin–d(C-A-T-G) complex in aqueous solution. This view emphasizes the conformation of the cyclic decadepsipeptide backbone.

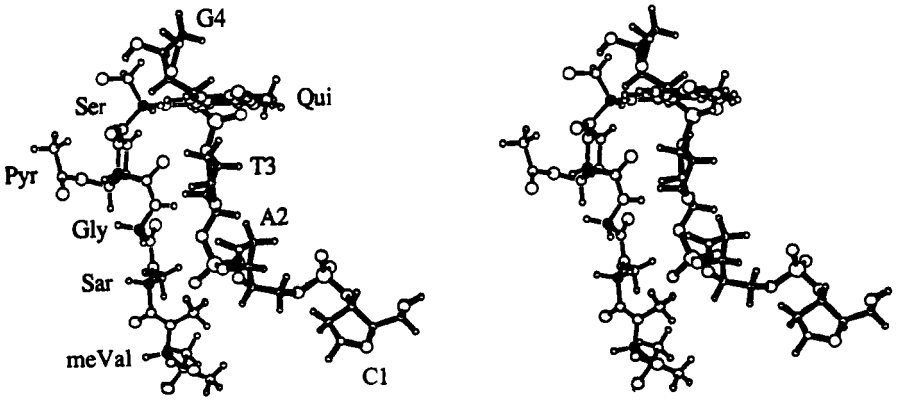

FIGURE 9: Stereopair establishing the complementary fit between the cyclic depsipeptide backbone of luzopeptin and the sugar–phosphate backbone of d(C-A-T-G) in the complex. The luzopeptin backbone is on the left and extends from the Ser$C\beta$ atom to the meVal $C\alpha$ atom and includes the quinoline chromophore. The amino acid positions are labeled next to the darkened $C\alpha$ atoms. The nucleic acid sugar–phosphate backbone (darkened bonds) is on the right with the bases deleted for clarity. The nucleic acid positions are labeled next to the sugar residues.

the $C\beta H_2$ protons are positioned opposite the minor-groove face of the G4 sugar in the complex. The pyridazine ring is positioned approximately opposite the sugar ring of T3 and its $C\delta H$ protons are directed toward the minor-groove face of the T3 sugar in the complex. The NCH_3 group of Sar, which is positioned in the plane and projects outward from the cyclic depsipeptide ring, is directed toward the sugar–phosphate backbone at the A2-T3 step in the complex. The NCH_3 group of L-meVal, which is normal to the cyclic depsipeptide plane and projects toward the DNA, is part of a hydrophobic cluster that includes the minor-groove face of the A2 sugar and the hydrophobic edge of the quinoline ring in the complex.

The pyridazine CαH, sarcosine $C\alpha H_2$, and glycine $C\alpha H_2$ protons are directed toward the interior of the cyclic depsipeptide backbone, and this hydrophobic patch is positioned opposite the minor-groove edge of the internal A2·T3 base pairs in the complex.

Thus, a combination of intermolecular hydrogen bonds and van der Waals contacts stabilize the complementary interactions between the cyclic depsipeptide backbone of luzopeptin and the minor-groove surface of the d(C-A-T-G) duplex in the NMR–MD-refined structure of the complex in solution.

Discussion

Previous Research on the Luzopeptin–DNA Complex. An earlier two-dimensional NMR study has reported on the nonexchangeable proton resonance assignments and intermolecular NOEs in the luzopeptin–d(G-C-A-T-G-C) complex (Searle et al., 1989). These authors concluded that luzopeptin bisintercalates in the minor groove at d(C-A)·d(T-G) sites with the quinoline rings sandwiching two base pairs on luzopeptin–d(G-C-A-T-G-C) complex formation (Searle et al., 1989). The present NMR studies on the luzopeptin–d(C-A-T-G) complex lend support to the earlier nonexchangeable proton assignments as well as the above qualitative conclusions on minor-groove recognition and the number of base pairs separated by the bisintercalating chromophores. These agreements notwithstanding, the present study extends the earlier research in several ways and through quantitative analysis of the experimental data defines the structure of the luzopeptin–DNA complex. Our structure of the luzopeptin–DNA complex has strinking differences from the earlier proposed model of Searle et al. (1989) based on a qualitative analysis of their NMR data sets. (1) The earlier NMR study was unable to assign the amide protons of D-Ser and Gly, as well as the $C\alpha H_2$ protons of Gly in the complex (Searle et al., 1989). This is a serious limitation since the assignment and characterization of NOEs involving the amide protons are critical for locating potential intermolecular hydrogen-bonding interactions in the luzopeptin–DNA complex. (2) The model of Searle et al. (1989) proposes that the critical conformational change on proceding from free luzopeptin to its DNA complex involves rotation of the Pyr-Gly amide group by 90° toward the DNA surface. However, as the authors themselves state in their concluding paragraph, they lack direct evidence for this rotation due to their inability to assign the Gly $C\alpha H_2$ protons. (3) The model of Searle et al. (1989) retains all trans peptide and ester bonds for luzopeptin on DNA complex formation. They were unable to monitor the CαH–CαH NOEs at the Pyr-Gly and Gly-Sar steps and hence were unable to differentiate between trans and cis orientations at these peptide linkages. Their conclusion of all trans peptide linkages contrasts dramatically with our demonstration of cis peptide bonds at the Pyr-Gly and Gly-Sar steps in the luzopeptin–d(C-A-T-G) complex. (4) Our NMR studies have emphasized the importance of NOEs involving exchangeable protons in defining the conformation of the luzopeptin–DNA oligomer complex. The sizable number of intermolecular NOEs deduced from the NOESY data set on the luzopeptin–d(C-A-T-G) complex in H_2O solution (Table VII, Figures 1 and S2) contrasts with the total absence of NOEs involving exchangeable protons in the luzopeptin–d(G-C-A-T-G-C) complex studied previously (Searle et al., 1989). (5) The earlier NMR research on the luzopeptin–DNA oligomer complex was limited to qualitative conclusions since Searle et al. (1989) did not attempt to measure interproton distance bounds and analyze them with structure reconstruction algorithms. By contrast, our use of NMR distance constraints as input parameters in a molecular dynamics computation has yielded a detailed three-dimensional view of the intermolecular interactions that account for the sequence specificity and stability of luzopeptin bisintercalated at d(C-A)·d(T-G) steps in the d(C-A-T-G) duplex.

Sequence Specificity. Our initial efforts focused on a comparative NMR study of luzopeptin complexes with the d(C-A-T-G) and d(C-T-A-G) self-complementary duplexes. We were able to generate a single complex in the case of the luzopeptin–d(C-A-T-G) complex (Figure S1), while the NMR spectra established a heterogenity of products when luzopeptin was added to the d(C-T-A-G) duplex. The NMR–MD structure of the luzopeptin–d(C1-A2-T3-G4) complex (Figure 6) is stabilized by a pair of symmetry-related intermolecular hydrogen bonds between the amide proton of Gly and the O2 carbonyl of T3 in the minor groove. The acceptor atom for the intermolecular hydrogen bond would have to be the N3 nitrogen of A3 in the luzopeptin–d(C1-T2-A3-G4) complex, and it appears to be a less than optimal interaction on the basis of the mixture of complexes observed experimentally.

Our studies demonstrate that intermolecular hydrogen-bond formation also explains the requirement for G·C base pairs to flank the quinoline at the bisintercalation site in luzopeptin–DNA complexes. The NMR–MD structure of the luzopeptin–d(C1-A2-T3-G4) complex is stabilized by a pair of symmetry-related intermolecular hydrogen bonds between the ester carbonyl of L-*N*-meVal and the 2-amino group of G4 in the minor groove. The intermolecular hydrogen-bonding capability of the guanosine 2-amino group has previously been shown to play a critical role in stabilizing the chromomycin–DNA complex (Gao & Patel, 1989a,b).

An interesting question relates to whether G·C base pairs can be sandwiched instead of A·T pairs by the quinolines at the bisintercalation site in the NMR–MD structure of the luzopeptin–DNA oligomer complex derived in this study. In other words, is there enough room in the minor groove at the intermolecular surface to replace the H2 of A by the NH_2 of G without disruption of the complex? An examination of the NMR–MD structure of the luzopeptin–d(C1-A2-T3-G4) complex establishes that there is sufficient room to replace the adjacent A2·T3 base pairs by G2·C3 base pairs. We believe that luzopeptin preferentially complexes to d(C1-A2-T3-G4) over d(C1-G2-C3-G4) due to a complementary intermolecular hydrophobic interaction between the CαH protons of Pyr, Gly, and Sar on luzopeptin and the H2 proton of A2, which is lost on replacement by the NH_2 group of G2.

We note that both amide protons of Gly and Ser exchange slowly and are shielded from solvent in the luzopeptin–d(C-A-T-G) complex in solution. The slow exchange of the Gly amide proton reflects its participation in an intermolecular hydrogen bond in the complex. The Ser amide proton does not form an intermolecular hydrogen bond in the NMR–MD structure of the luzopeptin–d(C-A-T-G) complex but rather is shielded from solvent in a hydrophobic environment at the intermolecular surface of the complex. Specifically, the Ser amide proton is in the plane formed by the quinoling ring and directed toward the NCH_3 group of L-*N*-meVal across the rectangular arrangement of the cyclic depsipeptide backbone of luzopeptin in the complex.

Trans to Cis Peptide Bond Isomerization. The most revealing insight that emerged from the current NMR–MD study of the luzopeptin–DNA complex is that the antitumor agents can undergo pronounced conformational transitions associated with their binding to target DNA. It has been known that cis peptide bonds can form at NCH_3-substituted

amino acids and proline residues such as at X-Pro and X-Sar steps in oligopeptides and proteins. The cyclic depsipeptide of luzopeptin contains Pyr, L-*N*-meVal, and Sar residues that lack an amide proton, as well as a glycine residue. Thus, cis peptide bonds can potentially form at Ser-Pyr, Pyr-Gly, Gly-Sar, and Sar-meVal peptide linkages in luzopeptin. Experimentally, the peptide bonds are all trans at these positions in free luzopeptin in the crystal (Arnold & Clardy, 1981) but switch to cis peptide bonds at Pyr-Gly and Gly-Sar on formation of the luzopeptin–d(C-A-T-G) complex in solution.

The starting Init-A (Figure 5A) and Init-B (Figure 5B) conformations of the complex had all trans peptide bonds and there was no bias in favor of cis peptide linkages at specific steps. Rather, the intramolecular (Table V) and intermolecular (Tables VI and VII) distance bounds estimated from the NOE intensities were only satisfied in the molecular dynamics calculations when the Pyr-Gly and Gly-Sar peptide bonds of luzopeptin in the complex underwent a trans to cis isomerization. Such trans to cis peptide bond isomerizations are part of the global search of the XPLOR molecular dynamics program in its attempt to deduce low-energy conformations that satisfy the experimental distance constraints.

We are aware of limitations in the NMR–MD analysis that arise as a consequence of the 2-fold symmetry element that relates the symmetrical halves of luzopeptin in both the free drug and its complex with the self-complementary d(C-A-T-G) duplex. Thus, in the absence of specific labeling it is not possible to distinguish whether an observed NOE between the CαH protons of Pyr and Gly originates between neighboring residues in the sequence or the same residues across the rectangular arrangement of the cyclic depsipeptide ring of luzopeptin. The observation of cis peptide bonds in the NMR–MD structure of the luzopeptin–d(C-A-T-G) complex is based on the assignment of the strong NOEs to CαH protons on adjacent residues rather than the same residues across the cyclic depsipeptide backbone. Our global search in the molecular dynamics simulations did not yield structures of the complex that satisfied the distance constraints where the short CαH–CαH distances between Pyr and Gly and between Gly and Sar arose from cross-strand interactions.

Comparison of Nogalamycin and Luzopeptin Intercalation Sites. The antitumor antibiotic nogalamycin intercalates through its aglycon ring at d(C-A)·d(T-G) steps in duplex DNA such that the nogalose sugar is positioned in the minor groove and the bicyclic amino sugar is positioned in the major groove (Searle et al., 1988b; Zhang & Patel, 1990). It is instructive to compare the structure of the common d(C-A)·d(T-G) intercalation sites in the NMR–MD-refined structure of the nogalamycin–d(A-G-C-A-T-G-C-T) complex (Zhang & Patel, 1990) with the NMR–MD-refined structure of the luzopeptin–d(C-A-T-G) complex (this study). One expects the structure of the intercalation sites to be different since the long axis of the intercalating aglycon of the nogalamycin is aligned orthogonal to the long axis of the flanking base pairs (Zhang & Patel, 1990), while the long axis of the intercalating quinoline rings of luzopeptin are aligned parallel to the long axis of the flanking base pairs (this study). The expected structural differences are indeed observed, with the base pairs buckled at the nogalamycin intercalation site, resulting in a wedge-shaped alignment of C and A on the C-A strand, compared to a parallel alignment of T and G on the T-G strand in the complex (Zhang & Patel, 1990). By contrast, no buckling of base pairs is detected at the luzopeptin bisintercalation site with a parallel alignment of A·T and G·C base pairs flanking the intercalated quinoline chromophores in the complex (this study). We have reported previously on a pronounced shearing of the base pairs relative to each other at the intercalation site in the nogalamycin–DNA complex, such that there is a strong overlap between the T and G bases on one strand while there is no overlap between C and A bases on the partner strand (Zhang & Patel, 1990) (Figure S8B, supplementary material). We also detect shearing of the base pairs at the luzopeptin bisintercalation site (this study), but this feature is less pronounced in the luzopeptin complex (Figure S8A) compared to the nogalamycin complex (Figure S8B). These comparisons establish that the geometry of the d(C-A)·d(T-G) intercalation site can be modulated by the orientation and overlap geometry of the intercalating chromophore, and hence the DNA is flexible enough to accommodate a range of intercalation sites.

Comparison of Echinomycin and Luzopeptin Bisintercalation Complexes. The antitumor antibiotics echinomycin and luzopeptin are both bisintercalating agents with the chromophores (quinoxaline for echinomycin and quinoline for luzopeptin) attached to bicyclic (echinomycin) or cyclic (luzopeptin) depsipeptide backbones. Footprinting (Van Dyke & Dervan, 1984; Low et al., 1984), X-ray (Wang et al., 1984), and NMR (Gao & Patel, 1988) studies have established that the echinomycin quinoxaline chromophores bisintercalate through the minor groove and sandwich two G·C base pairs between them at d(C-G)·d(C-G) sites. By contrast, the luzopeptin quinoline chromophores bisintercalate through the minor groove and sandwich two A·T base pairs between them at d(A-T)·d(A-T) sites (Searle et al., 1989; this study). It has been established that the sandwiched G·C pairs adopt Watson–Crick alignments in the echinomycin complexes (Wang et al., 1984; Gao & Patel, 1988), and the sandwiched A·T pairs adopt Watson–Crick alignments in the luzopeptin complexes (Searle et al., 1989; this study).

A pair of symmetrical intermolecular hydrogen bonds between the amide proton of Ala and the guanosine N3 of the sandwiched Watson–Crick G·C pair in the minor groove stabilizes the echinomycin–DNA complex (Wang et al., 1984; Gao & Patel, 1988) and contributes to the sequence specificity of the binding. Similarly, a pair of symmetrical intermolecular hydrogen bonds between the amide proton of Gly and the O2 of the thymidine of the sandwiched Watson–Crick A·T pair in the minor groove stabilizes the luzopeptin–DNA complex (this study) and contributes to the sequence specificity of the binding.

It has been established that the base pairs on either side of the echinomycin bisintercalation site adopt Hoogsteen pairing in the crystalline state (Wang et al., 1984). By contrast, NMR studies in solution have established that sequence (Gao & Patel, 1988), pH (Gao & Patel, 1989b), temperature (Gilbert et al., 1989), and length (Gao & Patel, 1989b) modulate whether the base pairs on either side of the echinomycin binding site adopt Watson–Crick or Hoogsteen pairing. We note that the G·C base pairs flanking the bisintercalation site adopt Watson–Crick alignments in luzopeptin complexes with the d(C-A-T-G) duplex (this study), the d(G-C-A-T-G-C) duplex (Searle et al., 1989), and the d(C-C-C-A-T-G-G-G) duplex (Zhang, Radhakrishnan, and Patel, in preparation).

Summary. This study reports on a combined NMR–molecular dynamics characterization of the solution structure of the luzopeptin–d(C-A-T-G) complex. The quinoline chromophores of luzopeptin bisintercalate at d(C-A)·d(T-G) steps and sandwich two A·T base pairs at the minor-groove binding site. The A·T and G·C base pairs retain Watson–Crick alignments, with the quinoline rings stacking with both A2

and G4 at the intercalation site. A set of specific intermolecular hydrogen bonds and hydrophobic interactions accounts for the specificity of luzopeptin for its preferred d(C-A-T-G)·d(C-A-T-G) binding site on duplex DNA.

Our structure of the luzopeptin–d(C-A-T-G) complex, which was based on 96 intermolecular distance constraints, establishes that the bound luzopeptin has cis peptide bonds at Pyr-Gly and Gly-Sar linkages in contrast to all trans peptide bonds in free luzopeptin in the crystalline state (Arnold & Clardy, 1981). These conclusions differ significantly from an earlier NMR-based structure of the luzopeptin–d(G-C-A-T-G-C) complex (Searle et al., 1989), where luzopeptin essentially binds in the conformation (all trans peptide bonds) found in the crystal structure of the free antibiotic. The investigation of Searle et al. (1989) was based on fewer intermolecular NOEs involving nonexchangeable protons only (total of 36) and was limited by the authors' inability to assign Gly amide and $C\alpha H_2$ protons and Ser amide protons in the complex. No attempt was made in the earlier study to quantitate the NOE data by using structure reconstruction algorithms (Searle et al., 1989).

The present characterization of the luzopeptin–DNA complex coupled with earlier investigations of the echinomycin–DNA complex (Gao & Patel, 1988) and the ditercalinium–DNA cmoplex (Delepierre et al., 1989; Maroun et al., 1989) provide novel insights into the recognition of the DNA duplex by natural and synthetic bisintercalating agents.

Supplementary Material Available

Figures S1–S8, showing one-dimensional NMR spectra of the complex in H_2O and D_2O, a 150-ms mixing time NOESY contour plot of the complex in H_2O, expanded COSY contour plots of the complex in H_2O and D_2O, NOESY contour plots of the complex in D_2O, expanded COSY contour plots of the complex in D_2O, stereopairs of free luzopeptin in the crystal and luzopeptin in the complex in solution, stereopairs of the Pyr-Gly-Sar segment in free luzopeptin in the crystal and luzopeptin in the complex in solution, and stereopairs of the overlap geometry at the (C-A)·(T-G) intercalation site in luzopeptin–DNA and nogalamycin–DNA complexes in solution (10 pages). Ordering information is given on any current masthead page.

References

Arnold, E., & Clardy, J. (1981) *J. Am. Chem. Soc. 103*, 1243–1244.

Borgias, B. A., & James, T. L. (1988) *J. Magn. Reson. 79*, 493.

Brooks, B. R., Bruccoleri, R. E., Olafson, B. D., States, D. J., Swaminathan, S., & Karplus, M. (1983) *J. Comput. Chem. 4*, 187–217.

Clore, G. M., & Gronenborn, A. M. (1984) *FEBS Lett. 172*, 219–225.

Clore, G. M., Nilges, M., Sukumaran, D. K., Brunger, A. T., Karplus, M., & Gronenborn, A. M. (1986) *EMBO J. 5*, 2727–2735.

Delepierre, M., Huynh Dinh, T., & Roques, B. P. (1989) *Biopolymers 28*, 2115–2142.

Fox, K. R., Davies, H., Adams, G. R., Portugal, J., & Waring, M. J. (1988) *Nucleic Acids Res. 16*, 2489–2507.

Gao, X., & Patel, D. J. (1988) *Biochemistry 27*, 1744–1751.

Gao, X., & Patel, D. J. (1989a) *Biochemistry 28*, 751–762.

Gao, X., & Patel, D. J. (1989b) *Q. Rev. Biophys. 22*, 93–138.

Gilbert, D. A., van der Marel, G. A., van Boom, J. H., & Feigon, J. (1989) *Proc. Natl. Acad. Sci. U.S.A. 86*, 3006–3010.

Gronenborn, A. M., & Clore, G. M. (1985) *Prog. Nucl. Magn. Reson. Spectrosc. 17*, 1–33.

Gronenborn, A. M., Clore, G. M., & Kimber, B. J. (1984) *Biochem. J. 221*, 723–736.

Hare, D. R., Wemmer, D. E., Chou, S. H., Drobny, G., & Reid, B. R. (1983) *J. Mol. Biol. 171*, 319–336.

Huang, C. H., Mong, S., & Crooke, S. T. (1980) *Biochemistry 19*, 5537–5542.

Huang, C. H., Prestayko, A. W., & Crooke, S. T. (1982) *Biochemistry 21*, 3704–3710.

Huang, C. H., Mirabelli, C. K., Mong, S. K., & Crooke, S. T. (1983) *Cancer Res. 43*, 2718–2724.

Konishi, M., Ohkuma, H., Sakai, F., Tsuno, T., Koshiyama, H., Naito, T., & Kawaguchi, H. (1981) *J. Am. Chem. Soc. 103*, 1241–1242.

Lane, A. M. (1988) *J. Magn. Reson. 78*, 425.

Low, C. M., Drew, H. R., & Waring, M. J. (1984) *Nucleic Acids Res. 12*, 4865–4879.

Maroun, R., Delepierre, M., & Roques, B. P. (1989) *J. Biomol. Struct. Dyn. 7*, 607.

Nerdal, W., Hare, D. R., & Reid, B. R. (1988) *J. Mol. Biol. 201*, 717–739.

Ohkuma, H., Sakai, F., Nishiyama, Y., Ohbayashi, M., Imanishi, H., Konishi, M., Koshiyama, H., & Kawaguchi, H. (1980) *J. Antibiot. 33*, 1087–1097.

Reid, B. R., Banks, K., Flynn, P., & Nerdal, W. (1989) *Biochemistry 28*, 10001–10007.

Rose, W. C., Schwig, J. E., Huftalen, J. B., & Bradner, W. T. (1983) *Cancer Res. 43*, 1504–1510.

Ryckaert, J. P., Cicotti, G., & Berendson, H. J. (1977) *J. Comput. Phys. 23*, 327–337.

Searle, M. S., Hall, J. G., & Wakelin, L. P. (1988a) *Biochem. J. 256*, 271–278.

Searle, M. S., Hall, J. G., Denny, W. A., & Wakelin, L. P. (1988b) *Biochemistry 27*, 4340–4349.

Searle, M. S., Hall, J. G., Denny, W. A., & Wakelin, L. P. (1989) *Biochem. J. 259*, 433–441.

Tomita, K., Hoshimo, Y., Sasihara, T., & Kawaguchi, H. (1980) *J. Antibiot. 33*, 1098–1102.

Van Dyke, M. M., & Dervan, P. B. (1984) *Science 225*, 1122–1127.

Verlet, L. (1976) *Phys. Rev. 159*, 98–105.

Wang, A. H., Ughetto, G., Quigley, G. J., Hokoshima, T., van der Marel, G. A., van Boom, J. H., & Rich, A. (1984) *Science 225*, 1115–1121.

Waring, M. J., & Fox, K. R. (1983) in *Molecular Aspects of Anti-Cancer Drug Action* (Neidle, S., & Waring, M. J., Eds.) Macmillan, New York, pp 127–156.

Zhang, X., & Patel, D. J. (1990) *Biochemistry 29*, 9451–9466.